https://doi.org/10.5194/egusphere-2026-5595
Preprint. Discussion started: 22 September 2026

Airborne measurements and model evaluation of dimethyl sulfide over the Amazon rainforest and Pacific Ocean

Bianca E. Krumm [1,4], Matthias Kohl [1], Anna Martin [1], Joseph Byron [1], Alexandra Gutmann [1], Michael Hewson [2], Jos Lelieveld [1,3], Andrea Pozzer [1,3], and Jonathan Williams [1,3]

[1]Department of Atmospheric Chemistry, Max Planck Institute for Chemistry, Mainz, Germany
[2]Central Queensland University, Rockhampton, Australia
[3]Climate and Atmosphere Research Center, The Cyprus Institute, 1645 Nicosia, Cyprus
[4]now at: Institute of Climate and Energy Systems: Troposphere (ICE-3), Forschungszentrum Jülich, Jülich, Germany

Correspondence: Bianca E. Krumm (b.krumm@fz-juelich.de) and Jonathan Williams (jonathan.williams@mpic.de)

Abstract. Dimethyl sulfide (DMS) is the primary natural source of reduced sulfur to the atmosphere and, as a precursor to sulfate aerosols, indirectly influences Earth's climate. Despite its global significance, upper tropospheric DMS measurements, particularly in deep-convective outflows, remain limited. Here we present two airborne datasets of in-situ DMS observations spanning 0.3–14 km over the Amazon rainforest and eastern Indo-Pacific Ocean, obtained during the CAFE-Brazil and CAFE-Pacific campaigns. These measurements confirm an east-west decreasing concentration gradient in the Amazonian boundary layer and reveal frequent elevated DMS (up to 56 pptv) in marine upper tropospheric convective outflows. Model-observation comparisons were performed with the EMAC (ECHAM5/MESSy2 Atmospheric Chemistry) model using several marine and terrestrial emission inventories and three different convection parametrisations. The sole available global terrestrial inventory (Spiro et al., 1992) overestimates Amazonian DMS by approximately a factor of three. Among the marine DMS climatologies, the Hulswar et al. (2022) inventory provides the closest agreement with the measurements, although further refinements remain necessary. Of the convection schemes tested, the Tiedtke scheme with Nordeng closure best reproduces the observed vertical DMS profile. Our results highlight the need for improved DMS emission parametrisations and show that the choice of convection scheme strongly influences the representation of the atmospheric sulfur cycle in global models. The frequent occurrence of DMS in deep convective outflow underscores the importance of further investigations into its transport, oxidation at cold temperatures, and role in new particle formation in the upper troposphere and stratosphere.

1 Introduction

Dimethyl sulfide (DMS) is the dominant natural source of reduced sulfur to the Earth's atmosphere, emitted mainly from the oceans with smaller contributions from terrestrial vegetation and soils (Andreae, 1990). In the atmosphere, DMS is oxidised to secondary sulfate aerosol, which influences climate both directly—by scattering and absorbing radiation (Charlson et al., 1991; Myhre et al., 2013)—and indirectly, by acting as a precursor for cloud condensation nuclei (CCN) that modify cloud albedo (Charlson et al., 1987; Ayers and Gras, 1991; Korhonen et al., 2008; Fiddes et al., 2018). It has been proposed that this mechanism could provide a negative feedback to global warming: as oceans warm, DMS emissions would increase, leading to

https://doi.org/10.5194/egusphere-2026-5595
Preprint. Discussion started: 22 September 2026

more reflective aerosol and clouds that cool the planet (Shaw, 1983; Charlson et al., 1987). Although anthropogenic fossil fuel combustion now dominates global sulfur emissions, natural sources still account for the bulk of atmospheric sulfate aerosol (Chin and Jacob, 1996). Therefore, a better understanding of the emission mechanisms and tropospheric distribution of natural sulfur sources, particularly DMS, and their representation in global climate models is essential for reducing uncertainties in indirect aerosol forcing (Carslaw et al., 2013).

DMS in surface waters is produced mainly by bacterial and algal degradation of dimethylsulfoniopropionate (DMSP), a phytoplankton metabolic product (Hopkins et al., 2023). Once dissolved, DMS can be (i) consumed by bacteria (Simó et al., 1998), (ii) photo-oxidised by UV radiation (Brimblecombe and Shooter, 1986; Galí et al., 2023), or (iii) emitted to the atmosphere. Sea-air exchange of DMS (and other trace gases) is controlled by the concentration gradient across the air-sea interface and by the surface wind speed (Liss and Slater, 1974; Mesarchaki et al., 2015). In the marine boundary layer, DMS shows a characteristic diel pattern: photochemical loss by OH radicals and boundary layer dynamics produce a midday minimum, while night-time accumulation leads to an early morning maximum (Andreae and Raemdonck, 1983; Nowak et al., 2001; Jackson et al., 2020). Numerous shipborne campaigns have measured DMS over the world's oceans in the tropics (Williams et al., 2004), mid-latitudes (Colomb et al., 2009), and the poles (Leck and Persson, 1996). In addition, aircraft campaigns have characterised the vertical distribution of DMS in the marine atmosphere (Thornton et al., 1997; Nowak et al., 2001; Conley et al., 2009; Marandino et al., 2013; Novak et al., 2021), yet observations of DMS that have been lofted to the upper troposphere (10–14 km) by deep convection remain scarce, because few research aircraft are capable of reaching those altitudes.

Terrestrial DMS emissions are dominated by biogenic sources, mainly from vegetation and soils with minor contributions from wetlands and salt marshes, and represent ~ 15% of the global DMS budget (Watts, 2000). Plant-derived DMS fluxes are controlled by photosynthetically active radiation (PAR) and temperature, and exhibit strong inter-species variability (Yonemura et al., 2005; Geng and Mu, 2006; Jardine et al., 2015; Vettikkat et al., 2020). Sulfur is an essential nutrient for plants, primarily taken up as sulfate through the roots (Droux, 2004), but it can also be absorbed from the atmosphere as gaseous sulfur compounds such as carbonyl sulfide (Li et al., 2024). It has been proposed that the emission of reduced sulfur gases serves as a mechanism for plants to dispose of excess sulfur (Rennenberg, 1984). However, the biochemical pathway responsible for primary DMS production in higher plants remains unresolved. Soil- and leaf litter-derived emissions have also been reported and are linked to microbial respiration, with temperature and soil moisture as the main drivers (Staubes et al., 1989; Kesselmeier and Hubert, 2002; Jardine et al., 2015; Pugliese et al., 2023). Anthropogenic activities have also been identified as DMS sources: agricultural cultivation of crops (Fall et al., 1988; Kanda et al., 1992, 1995; Loubet et al., 2022), and livestock farming (Williams et al., 1999; Filipy et al., 2006; Shaw et al., 2007; Kammer et al., 2020). The contribution of these anthropogenic emissions to the terrestrial DMS budget is small, but they can be of importance locally (Williams et al., 1999).

Ecosystem scale measurements in the Amazon rainforest reveal DMS mixing ratios reaching up to 80 pptv at canopy level, where a modest midday peak in the diel cycle above the canopy was reported (Jardine et al., 2015). Elevated mixing ratios (~ 5–10 pptv) at canopy level have also been reported from temperate forests (Berresheim and Vulcan, 1992; Vermeuel et al., 2023). The lower-tropospheric DMS vertical distribution over the Amazon Basin was previously characterised by two aircraft campaigns in the 1980s (Andreae and Andreae, 1988; Andreae et al., 1990), yet no observations exist for the upper troposphere.

https://doi.org/10.5194/egusphere-2026-5595
Preprint. Discussion started: 22 September 2026

Once emitted into the atmosphere, DMS undergoes complex oxidation pathways involving gas- and liquid-phase reactions with radicals such as hydroxyl (OH), bromine oxide (BrO), bromine (Br), chlorine (Cl), and nitrate (NO_3) (Barnes et al., 2006; Hoffmann et al., 2016), resulting in a global mean atmospheric lifetime of 1-2 days (Chen et al., 2018). These reactions generate, among other products, methanesulfonic acid (MSA) and sulfuric acid (H_2SO_4), both of which are low-volatility species that are involved in new particle formation and growth of sulfate aerosol (Sipilä et al., 2010; Rasmussen et al., 2022). DMS-derived sulfate aerosol particles constitute an important source of CCN in the marine atmosphere (Korhonen et al., 2008).

Accurate global modelling of DMS is essential for quantifying the Earth's radiative budget (Fiddes et al., 2018), yet it remains challenging for several reasons. First, the emission mechanisms are complex and highly variable in space and time. Although multiple global sea water DMS inventories have been produced using different approaches (Kettle et al., 1999; Lana et al., 2011; Galí et al., 2018; Wang et al., 2020; Hulswar et al., 2022; Zhou et al., 2024), capturing mesoscale variability is still difficult (Bell et al., 2021; Salignat et al., 2025). In contrast, for terrestrial emissions, only a single inventory (Spiro et al., 1992) exists, and it has scarcely been evaluated against measurements. Second, sea air exchange velocities differ among parametrisations, and this can dominate the emission uncertainty in some regions (Joge et al., 2024). Third, the atmospheric chemistry of DMS is still uncertain because oxidant concentrations, particularly BrO and dissolved OH in cloud droplets, are poorly constrained (Chen et al., 2018). Finally, shortcomings in convection parametrisations further affect model performance (Rybka and Tost, 2014), underscoring the need for systematic validation against observational datasets also for short-lived processes.

Here we present airborne, in-situ DMS measurements covering most of the tropospheric column (0.3–14 km) over the Amazon rainforest and the east Indo-Pacific Ocean during the Chemistry of the Air Field Experiment (CAFE) Brazil and CAFE-Pacific campaigns, respectively, aboard the High Altitude Long Range (HALO) research aircraft. As the majority of flight time was dedicated to the upper troposphere and to sampling deep convective events, this dataset provides new insight into the vertical distribution of DMS, especially within rarely explored deep convective outflows. We also examine the spatial DMS patterns in both regions and compare them with the state-of-the-art global atmospheric chemistry model EMAC, focusing on how current marine and terrestrial emission climatologies represent DMS sources. Finally, we evaluate EMAC's ability to reproduce the observed vertical DMS distribution above the Pacific by testing three different global model convection parametrisations.

2 Methods

2.1 CAFE field missions

The measurements reported here were obtained aboard the HALO research aircraft during the Chemistry of the Atmosphere (CAFE) campaigns CAFE-Brazil (2022–2023), and CAFE-Pacific (2024).

The CAFE-Brazil campaign (Dec 2022–Jan 2023) operated from Manaus during the dry-to-wet transition. DMS was measured on 13 of the 16 research flights (RFs) over the Amazon Basin, providing the high vertical and spatial coverage shown in Figure 1. This mission aimed to investigate the atmospheric processing of biogenic rainforest emissions under conditions of strong convection and low biomass-burning activity (Machado et al., 2004; Tripathi et al., 2025).

https://doi.org/10.5194/egusphere-2026-5595
Preprint. Discussion started: 22 September 2026

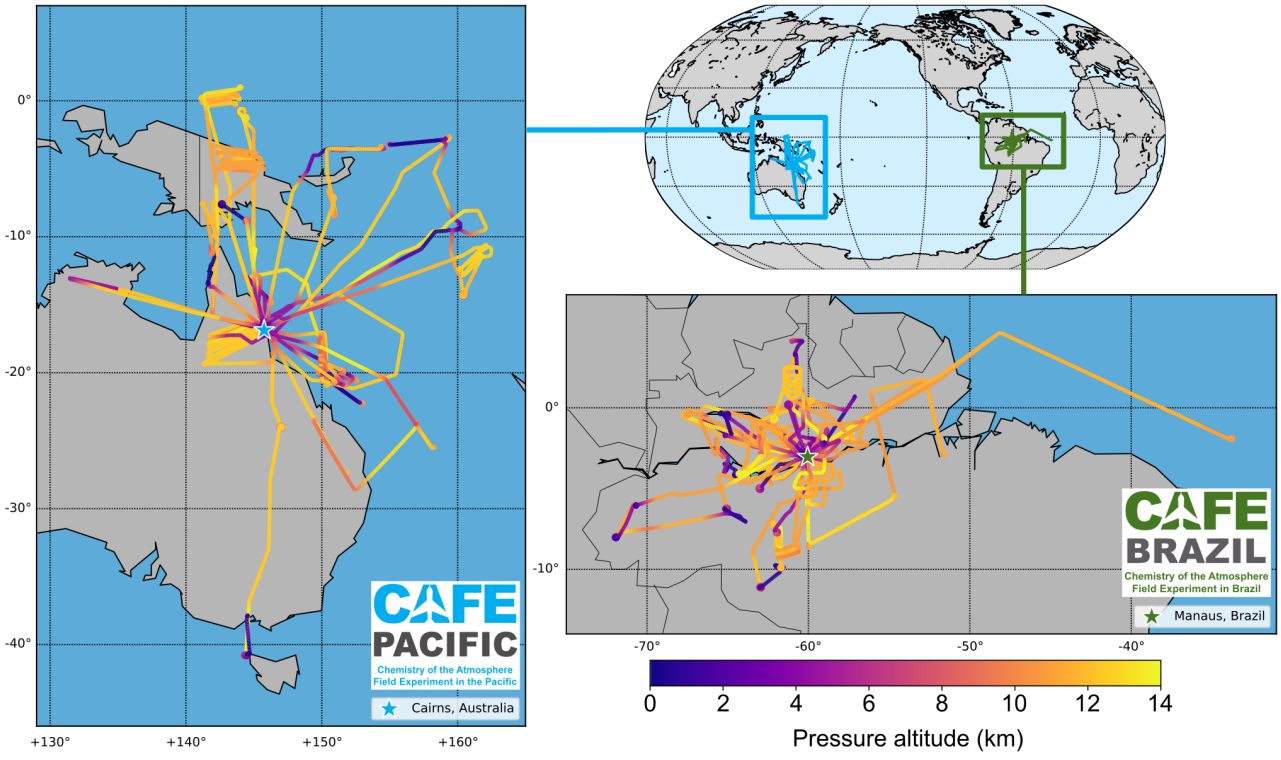

Figure 1. Flight tracks of the HALO aircraft for the CAFE-Brazil (Dez 22–Jan 23) and CAFE-Pacific (Jan–Feb 2024) campaigns, colour coded by altitude. Only those flights for which DMS measurements from the SOFIA instrument are available are shown. Campaign logos were designed by Tanja Pallien.

The CAFE-Pacific campaign (January–February 2024) took place during the Australian summer monsoon, a period characterised by high convective activity in the studied region (Pope et al., 2008). DMS was measured on 14 of the 18 RFs, sampling different regions of the east Indo-Pacific Ocean, including the Coral Sea, Bismarck Sea, Solomon Sea, and the Indo-Pacific Warm Pool, as well as continental air masses above Papua New Guinea and Australia (Figure 1).

2.2 Instrumentation

Airborne in-situ measurements of dimethyl sulfide (DMS) were conducted with a custom-made Fast Gas Chromatography-Mass Spectrometer (Fast GC-MS) instrument called System for Organic Fast Identification Analysis (SOFIA) aboard the High Altitude Long Range (HALO) research aircraft. The custom-made system has been described in detail elsewhere (Bourtsoukidis et al., 2017), as well as its configuration within the CAFE payload aboard HALO (Voigt et al., 2022).

Briefly, ambient air was drawn through the Trace Gas Inlet (TGI, Enviscope GmbH) and conveyed to the instrument via a heated PFA line (2 m, 0.6 cm o.d., 40°C) equipped with an ozone scrubber (Ernle et al., 2023). Within the inlet assembly,

https://doi.org/10.5194/egusphere-2026-5595
Preprint. Discussion started: 22 September 2026

the air was compressed to standard pressure (1 atm) at a flow rate of 200 sccm. Blank samples were generated by thermal decomposition of VOCs over a platinum catalyst (Pt/Al_2O_3, 3.2 mm pellets, Sigma-Aldrich) at 350°C in the Zero-Air-Generator. A gravimetrically prepared Calibration Standard (~ 50 ppbv VOCs in N_2, 5% stated uncertainty, Apel Riemer Environmental Inc.) was diluted with zero air to prepare calibration samples. The inlet system was constructed entirely from uncoated stainless steel tubing (0.6 cm o.d.). The total residence time of air between the TGI and the sampling point was approximately 15 s (Bourtsoukidis et al., 2017).

The sample stream was drawn from the inlet system at 40 sccm and passed through a series of cold traps, where it was dried at -10°C, cryogenically pre-concentrated for 1 min at -160°C, and finally re-focused at -160°C before injection into the GC. VOCs were separated on a mid-polarity capillary column (10 m x 0.25 mm i.d., 1.40 μm film thickness, DB-624 UI, Agilent Technologies). The custom-made GC oven was programmed as follows: hold at 30°C during the first 50 s, ramp at 1.8°Cs^{-1} to 200°C, then maintain 200°C until the end of the run after 144 s. After chromatographic separation, the VOCs were ionised by electron impact at -70 eV and detected with a quadrupole mass spectrometer (Agilent Technologies 5973 MSD) operating in selected ion monitoring (SIM) mode. The SIM method employed during the CAFE campaigns enabled the separation and quantification of >35 VOCs, including DMS, which eluted at 49.0 s (detected at $m/z = 62$). In this configuration, the instrument provided one data point every 3 minutes. 1860 airborne, ambient samples (equivalent to approx. 93 flight hours) were collected during CAFE-Brazil, and 1810 samples (approx. 91 flight hours) during CAFE-Pacific.

Full five-point calibrations were typically carried out on the ground before and after each research flight (RF). During flight, blank and calibration samples were measured at roughly hourly intervals to monitor the background signal and sensitivity.

Peak integration was carried out with the in-house MPIC-Chrom software (version 7) written in IGOR (Wavemetrics). During the data processing, we identified an interference caused by the water content of the samples, which affected the instrument's sensitivity. Consequently, this effect on the DMS signal was corrected by normalising to the area of the nearby CFC-113 peak (see Appendix A for details on the correction). The total uncertainty was derived by error propagation based on the given accuracy of the individual components (2–15% mass-flow controllers, 5% calibration gas standard, 0.5% sample volume, 0.1–10% peak fitting) and additional uncertainty from the correction (see Appendix A).

SOFIAs limit of detection (LOD) for DMS, defined as three times the standard deviation of the blank measurements, was 1.42 pptv during CAFE-Brazil and 1.63 pptv during CAFE-Pacific. The relative total uncertainty of DMS mixing ratios was ~ 40% for values between 3*LOD and 10*LOD, and ~ 20% for values higher than 10*LOD, while the precision was better than 5%. The aircraft's altitude and position, along with basic meteorological parameters were provided by the Basis HALO Measurement and Sensor System (BAHAMAS) (Giez et al., 2022).

2.3 EMAC model setup

Numeric simulations were performed with the ECHAM/MESSy Atmospheric Chemistry (EMAC) model, a numerical chemistry and climate simulation system that includes sub-models describing tropospheric and middle atmosphere processes and their interaction with oceans, land and human influences (Jöckel et al., 2010). It uses the second version of the Modular Earth Submodel System (MESSy2) to link multi-institutional computer codes. The core atmospheric model is the 5th generation

https://doi.org/10.5194/egusphere-2026-5595
Preprint. Discussion started: 22 September 2026

Table 1. List of performed simulations for CAFE-Pacific.

Short Name	Marine Climatology	Terrestrial Climatology	Convection Scheme
L11	Lana et al. (2011)	Spiro et al. (1992)	Tiedtke (1989); Nordeng (1994)
W20	Wang et al. (2020)	Spiro et al. (1992)	Tiedtke (1989); Nordeng (1994)
H22 / TN	Hulswar et al. (2022)	Spiro et al. (1992)	Tiedtke (1989); Nordeng (1994)
E99	Hulswar et al. (2022)	Spiro et al. (1992)	Emanuel and Živković Rothman (1999)
B04	Hulswar et al. (2022)	Spiro et al. (1992)	ECMWF (Bechtold et al., 2004)

European Centre Hamburg general circulation model (ECHAM5) (Roeckner et al., 2006)). The physics subroutines of the original ECHAM code have been modularised and reimplemented as MESSy submodels and have continuously been further developed. Only the spectral transform core, the flux-form semi-Lagrangian large-scale advection scheme, and the nudging routines for Newtonian relaxation remain from ECHAM. For the present study, we applied EMAC (MESSy version 2.55.0) in the T63L90MA-resolution, i.e., with a spherical truncation of T63 (corresponding to a quadratic Gaussian grid of approx. 1.8°×1.8° in latitude and longitude) with 90 vertical hybrid pressure levels up to 0.01 hPa. Gas phase and heterogeneous chemistry were represented by the Mainz Isoprene Mechanism (MIM1) within the MECCA submodel (Jöckel et al., 2006; Pöschl et al., 2000; Sander et al., 2019). All reactions involving DMS are listed in Table B1. The configuration of the submodels follows the setup described in Kohl et al. (2023).

Following Jeuken et al. (1996), the tropospheric dynamics in the EMAC simulations are nudged toward the ERA5 meteorological reanalysis (Hersbach et al., 2020) from the European Centre for Medium-Range Weather Forecasts (ECMWF) to reproduce the observed day-to-day variability of tropospheric meteorology.

The simulations covered the period from 01 January 2022 to 31 January 2023 for CAFE-Brazil and from 01 January 2023 through 01 April 2024 for CAFE-Pacific, providing a full year for model spin-up in both model runs. For comparison with aircraft observations, model results sampled along the flight trajectories were extracted at every model timestep using the S4D submodel (Jöckel et al., 2010). In addition, complete three-dimensional output fields were stored at hourly resolution.

Marine DMS emissions in the model are parametrised as a function of surface wind speed, temperature and sea-water DMS concentration, derived from a climatology, following Pozzer et al. (2006). For the CAFE-Pacific campaign, we performed EMAC simulations with three different marine seawater DMS climatologies (Table 1). Lana et al. (2011) provides an observation-based interpolation of seawater DMS concentrations within biogeographic provinces and has been the standard inventory in global models for the past decade (L11). Wang et al. (2020) employs a parametrisation derived from an artificial neural network analysis that links seawater DMS to environmental proxies such as chlorophyll a, nutrients, sea-surface temperature, and other factors (W20). Hulswar et al. (2022) is an updated version of L11 that incorporates newer observations and refined interpolation methods (H22).

Terrestrial DMS emissions are derived directly from the Spiro et al. (1992) land-surface climatology, and sensitivity runs were performed with (S92), without (noTER) and with reduced (rdS92) terrestrial DMS emissions to assess their impact (Table 2).

https://doi.org/10.5194/egusphere-2026-5595
Preprint. Discussion started: 22 September 2026

Table 2. List of performed simulations for CAFE-Brazil.

Short Name	Marine Climatology	Terrestrial Climatology	Convection Scheme
S92	Hulswar et al. (2022)	Spiro et al. (1992)	Tiedtke (1989); Nordeng (1994)
noTER	Hulswar et al. (2022)	none	Tiedtke (1989); Nordeng (1994)
rdS92	Hulswar et al. (2022)	0.39*Spiro et al. (1992)	Tiedtke (1989); Nordeng (1994)

Additional sensitivity experiments were performed to assess how the choice of convection parametrisation influences the simulated vertical distribution of DMS. Three convection schemes were employed: the EMAC default Tiedke-Nordeng formulation (Tiedtke, 1989; Nordeng, 1994) (TN), the Emanuel and Živković-Rothman scheme (Emanuel and Živković Rothman, 1999) (E99), and the ECMWF scheme (Bechtold et al., 2004) (B04). Detailed descriptions of these convection schemes and their implementation in EMAC are provided by Tost et al. (2006) and references therein.

2.4 Satellite imagery

Aqua-MODIS ocean chlorophyll-a concentration data (OCI-Algorithm) was obtained via NASA's Ocean Color Earthdata (OB.DAAC) on 11 November 2025. To obtain the campaign average of chlorophyll-a concentrations, five 8-day, 4-km spatial resolution rasters were averaged into a single map with an ESRI ArcGIS Pro raster cell average function, altogether spanning a period from January 17 to 25 February 2024. Cloud top temperature (CTT) (Bureau Of Meteorology, 2024b) and cloud type (CT) (Bureau Of Meteorology, 2024a) data, at hourly temporal and 0.02°×0.02° spatial resolution, were obtained from the Himawari Geostationary Meteorological Satellite 8/9 and processed by the Australian Government Bureau Of Meteorology (2021).

3 Results and Discussion

3.1 Observations during the CAFE missions

3.1.1 Vertical and spatial distribution

Vertical profiles of DMS mixing ratios for the two campaigns are presented in Figure 2 a. In the lower troposphere (<1 km), the marine measurements are roughly an order of magnitude higher than those obtained over the Amazon rainforest, consistent with the predominance of marine sources in the global DMS budget (Andreae, 1990; Watts, 2000). In both environments, the mixing ratios decline approximately exponentially with altitude up to approx. 4 km, reflecting dilution by turbulent entrainment of cleaner air aloft and chemical loss (e.g., via reaction with OH). In the mid-troposphere (4–9 km), the median mixing ratios fall below the LOD, with only occasional elevated values that may result from mid-level detrainment. In the upper troposphere (9–14 km), the CAFE-Pacific data frequently exhibit enhanced DMS mixing ratios associated with deep-convective transport,

https://doi.org/10.5194/egusphere-2026-5595
Preprint. Discussion started: 22 September 2026

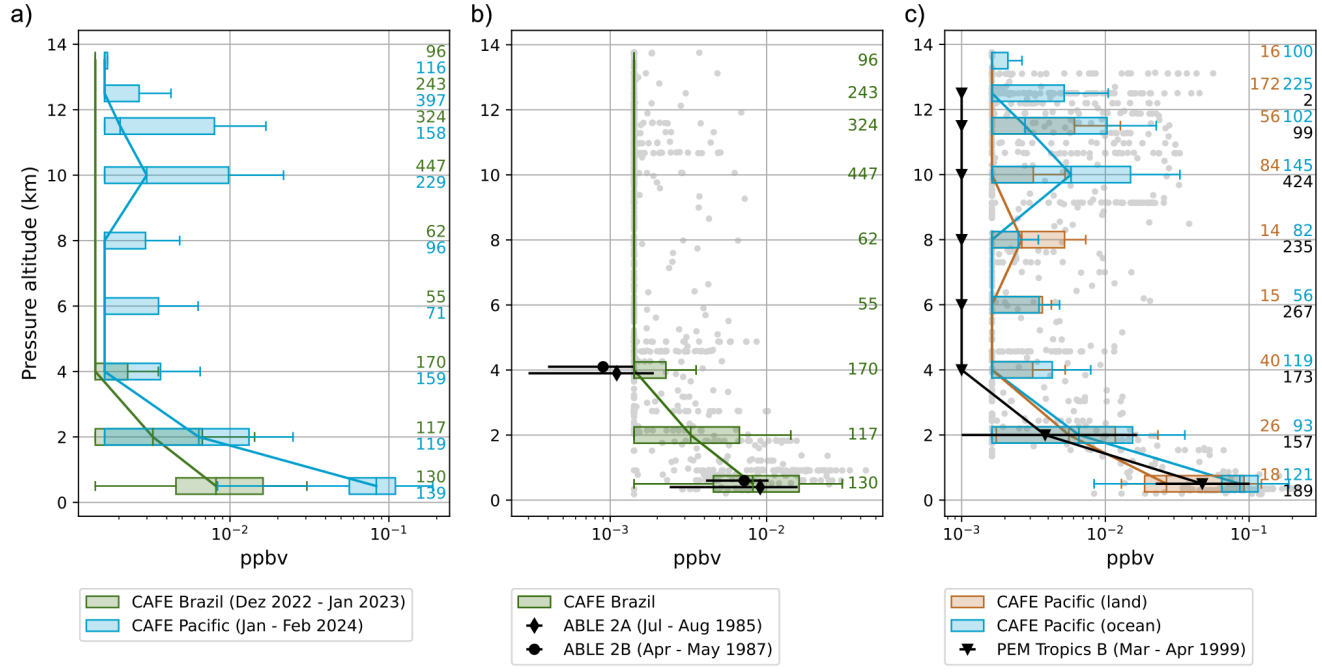

Figure 2. Vertical distribution of DMS volume mixing ratios. Values that fell below the LOD were set to the LOD. Data above 11 km were grouped into 1 km altitude bins because of the higher sampling density, whereas all remaining data were placed in 2 km bins; the number of observations in each bin is indicated on the right-hand side of the panels. The distributions are shown as box and whisker plots (25^{th}–75^{th} percentile boxes, median line), and in panels b) and c), the individual measurements are plotted in light grey. a) comparison of the CAFE-Brazil and CAFE-Pacific campaigns. b) CAFE-Brazil data together with measurements from the ABLE-2 campaign for two contrasting seasons (Andreae et al. (1990), Table 1). c) CAFE-Pacific data separated into over ocean and over-land points. The over ocean subset from the PEM-Tropics B campaign DC-8 measurements (Colman et al., 2001; Simpson et al., 2001; GTE Project Office et al., 2025) is overlaid for comparison (triangles represent median; errorbars indicate 25^{th}–75^{th} percentile range).

whereas only a few points above the Amazon exceed the LOD despite the occurrence of multiple deep-convective events (Curtius et al., 2024; Tripathi et al., 2025).

Figure 2 b compares the CAFE-Brazil vertical profile with the only two previous investigations of DMS vertical distribution above the Amazon Basin to the best of the authors' knowledge. Both studies were part of the Atmospheric Boundary Layer Experiment (ABLE) missions conducted with NASA's Electra aircraft in the 1980s and were limited to the lower troposphere (<6 km). The first campaign (ABLE-2A) was carried out at the onset of the dry season (July–August 1985; Andreae and Andreae (1988)), and the second (ABLE-2B) during the wet season (April–May 1987; Andreae et al. (1990)). In each season, the reported DMS mixing ratios were very similar, with slightly lower values in the wet season. Their boundary layer measurements agree remarkably well with our median value of 8.2 pptv below 1 km. In the free troposphere, the ABLE values lie just below our LOD, consistent with the fact that most of our observations in this altitude range are also below the LOD. Canopy

https://doi.org/10.5194/egusphere-2026-5595
Preprint. Discussion started: 22 September 2026

level measurements near Manaus reported diurnal mean mixing ratios of 14–22 pptv at 40 m altitude during December–January (Jardine et al., 2015), which likewise match the lower tropospheric values obtained in the present work. A comparable vertical distribution was observed above the Congolian rainforest during the DECAFE-88 campaign (Bingemer et al., 1992). Together, these independent datasets suggest that the DMS vertical profile reported here is consistent with previous observations in tropical rainforest environments over the past decades.

The spatial distribution of DMS mixing ratios below 1 km (Figure 3 a,b) shows a clear east-west gradient, with the highest values east of Manaus, nearer to the Atlantic coast and a systematic decrease toward the western Amazon. A comparable gradient was reported from the ABLE campaigns (Andreae and Andreae, 1988). In the lower troposphere over the Amazon basin east of Manaus, the prevailing wind was easterly, and west of Manaus, north-easterly (Figure 3 b). The sampled air masses were transported from the Atlantic coast toward the interior, typically within at least 2–3 days (Pöhlker et al., 2019). DMS from marine or coastal salt marsh origin could therefore contribute to the elevated eastern concentrations, although the transport time from the coast to the study region slightly exceeds the lower tropospheric atmospheric lifetime of DMS with respect to OH of approx. 1–1.5 days (Albu et al., 2006). To quantify the potential contribution of long-range transported marine DMS, we performed an EMAC simulation with marine emissions only (noTER; see Table 2). The model predicts mixing ratios up to 7 pptv and a north-south gradient, which is far smaller than the observed east-west gradient of ~ 20 pptv (Figure 3 c). Consequently, the gradient is likely mainly driven by spatial variations in terrestrial DMS emissions, with limited contributions from marine sources. The pronounced east-west gradient across Manaus aligns well with the gradient across recently identified Amazonian geoecological classes derived from floristic field data, satellite imagery, and climatic data, in which soil properties were found to be the primary driver (Tuomisto et al., 2019). This suggests that the Amazon rainforest may not be a uniform DMS source and that spatial variations in soil-related geoecological zones might influence DMS emissions.

The vertical profile for the CAFE-Pacific campaign, separated into over-land and over-ocean observations, is shown in Figure 2 c. Over-land, most measurements were obtained in the upper troposphere, with relatively few data points below 9 km. Furthermore, the lower tropospheric measurements over-land were primarily collected near the ocean and are likely influenced by marine emissions, making them unrepresentative of purely terrestrial conditions in the study region. In the upper troposphere over-land, DMS mixing ratios were generally below the LOD, consistent with the observations from CAFE-Brazil.

The over-ocean profile is compared in Figure 2 c with measurements from the Pacific Exploratory Mission (PEM) Tropics-B campaign aboard NASA's DC-8, which sampled the tropical Pacific during the wet season (March–April 1999) (Colman et al., 2001; Simpson et al., 2001; GTE Project Office et al., 2025). This dataset was selected because, among the available aircraft DMS measurements in marine regions, it provides the greatest overlap in region, season, and altitude range with our observations. Both profiles exhibit a comparable exponential decline of DMS mixing ratios with altitude in the lower troposphere. Our median values are slightly higher, likely reflecting the predominance of coastal sampling (e.g., above the biologically productive waters of the Great Barrier Reef), while PEM Tropics-B sampled more over open oligotrophic ocean waters. A pronounced discrepancy between the two datasets appears in the upper troposphere. During CAFE-Pacific, we repeatedly observed deep convectively transported DMS with mixing ratios up to 56 pptv between 9 and 14 km. In contrast, the PEM Tropics-B data at those altitudes, despite extensive sampling, never exceeded 5 pptv. The reasons for this discrepancy

https://doi.org/10.5194/egusphere-2026-5595
Preprint. Discussion started: 22 September 2026

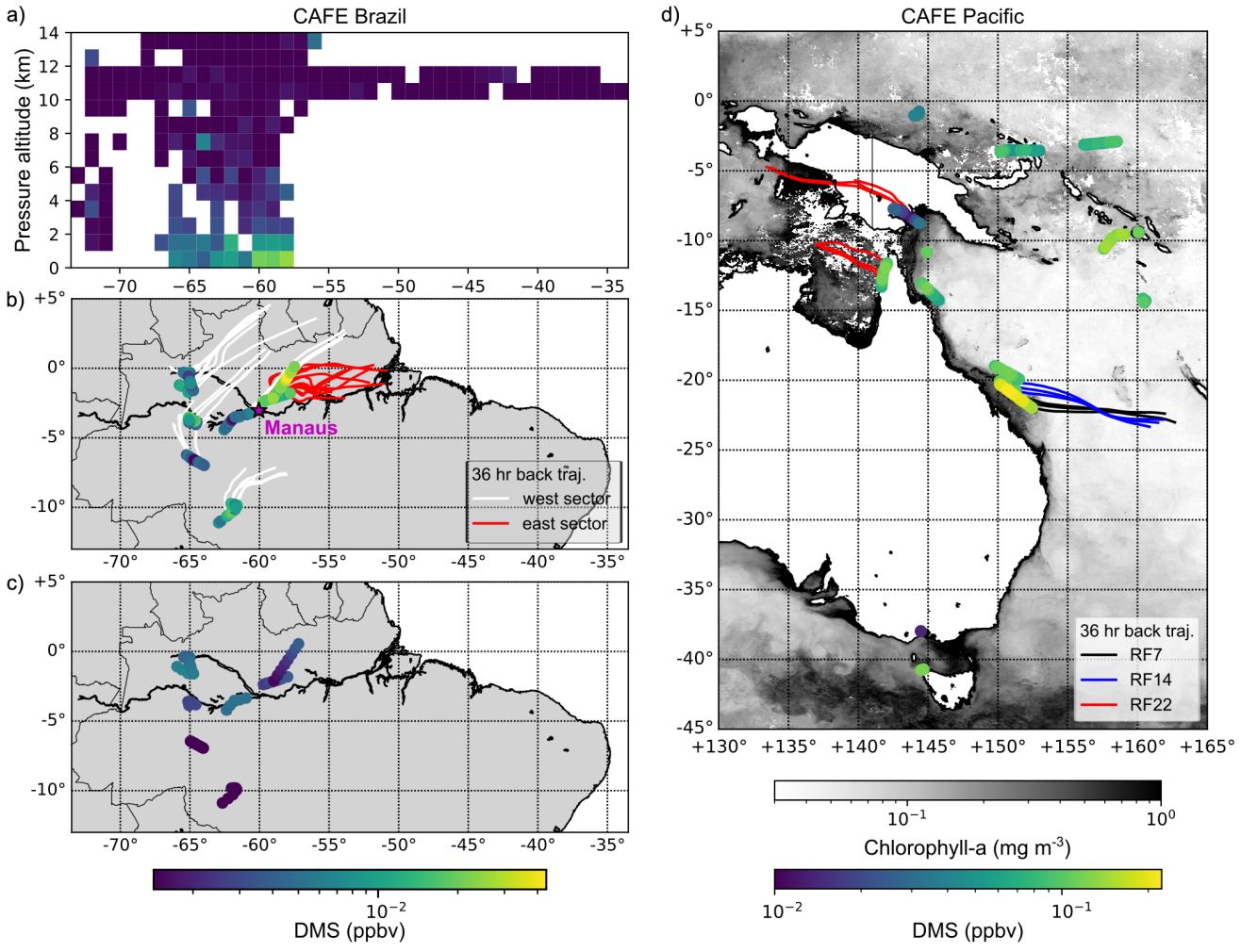

Figure 3. Spatial distribution of observed and modelled DMS volume mixing ratios during both campaigns. a) Longitudinal cross section of the CAFE-Brazil observations, mean values in a 1°x1 km latitude-altitude grid. b) CAFE-Brazil observed DMS mixing ratios at altitudes <1 km. c) CAFE-Brazil modelled DMS mixing ratios (<1 km) with marine emissions only (noTER). The colour scale for panels a)–c) is shown on the left. d) CAFE-Pacific measurements at altitudes <0.5 km, with its colour scale indicated on the right. The data is overlaid on an Aqua MODIS chlorophyll-a concentration map (average for the campaign period). 36 Hours back trajectories of selected points along the flight tracks were generated with the HYSPLIT transport and dispersion modelling system (Stein et al., 2015). Values below the LOD were replaced with the LOD.

https://doi.org/10.5194/egusphere-2026-5595
Preprint. Discussion started: 22 September 2026

are not clear. One possible explanation is differences in flight planning, as our campaign specifically targeted regions where deep convection was expected. To date, only a limited number of in-situ measurements of similarly elevated upper tropospheric DMS concentrations associated with convective uplift are available in the literature. Thornton et al. (1997) reported mixing ratios of up to 20 pptv (respectively 80 pptv during a typhoon) above 8.5 km altitude during the PEM West-A (September–October 1991) and B (February–March 1994) campaigns, which matches our observations. During the HIAPER Pole to Pole Observations (HIPPO) 2 campaign, elevated DMS levels around 100 pptv were found between 8-10 km (Marandino et al., 2013).

Figure 3 d displays the spatial distribution of DMS mixing ratios below 0.5 km during the CAFE-Pacific campaign. In the marine boundary layer (<1 km), the inter-quartile range (25–75 percentile) spans 65–115 pptv, with a median of 86 pptv. The highest value (223 ppt) was recorded during RF7 (21 January 2024, 12 h local time) at 0.35 km altitude above the Great Barrier Reef. By contrast, RF14 (15 Feburary 2024, 12 h local) sampled the same altitude, location and time of day but observed markedly lower mixing ratios (~ 100 ppt). Our HYSPLIT back-trajectory analysis shows that the air masses sampled on both flights originated from similar regions of the Coral Sea. Although the tropical cyclone Kirrily was present in the Coral Sea during RF7 (see next section), its closest approach to the trajectory was more than 700 km away, making a direct impact on the measured DMS concentrations, e.g., via enhanced surface windspeeds, unlikely. The measured wind speed was slightly higher on RF7 (8–9 m s^{-1}) than on RF14 (6–7 m s^{-1}), which may account for part of the difference. Overall, DMS mixing ratios in the marine boundary layer (<0.5 km) show modest positive correlations with wind speed (Pearson r = 0.43) and the decadic logarithm of ocean chlorophyll-a concentrations (Pearson r = 0.40) at the sampling location.

During RF22 (25 February 2024, 9 h local time), we sampled boundary layer air (~ 0.2 km) over mangrove and salt marsh habitats between Aurukun and Mapoon on the north west coast of Queensland. The airmasses were a mixture of local vegetation emissions (evidenced, e.g., by elevated isoprene levels) and a marine background, as they originated from the adjacent Gulf of Carpentaria. The mean DMS mixing ratio on this leg was 96 pptv, which falls well within the typical marine range and indicates that any contribution from the coastal wetlands was at most on the order of a few tens of pptv. This finding contrasts with the unusually large *m/z* 63 signal reported from a 1998 PTR-MS aircraft campaign over Surinam, which was interpreted as a DMS mixing ratio of 395 pptv in the forest boundary layer and attributed to strong emissions from coastal wetlands (Crutzen et al., 2000). The quadrupole mass spectrometer used in that study likely suffered from an interference at the DMS mass. In our extensive dataset, encompassing the Amazon rainforest with its numerous riverine wetlands, and the coastal wetlands of northern Australia, such elevated DMS concentrations are absent, indicating that intense DMS emissions from wetlands are either highly localised, episodic, or both.

3.1.2 In-situ observations of convective uplift into the upper troposphere

Although deep-convective transport of air masses was frequently observed over the Amazon rainforest (Curtius et al., 2024; Tripathi et al., 2025), the DMS measurements in those events were generally at or below the LOD, with only a few outliers. In contrast, elevated DMS mixing ratios associated with deep convection were encountered repeatedly in the marine upper troposphere above the Pacific Ocean. Below, we describe two of those convective events in detail.

https://doi.org/10.5194/egusphere-2026-5595
Preprint. Discussion started: 22 September 2026

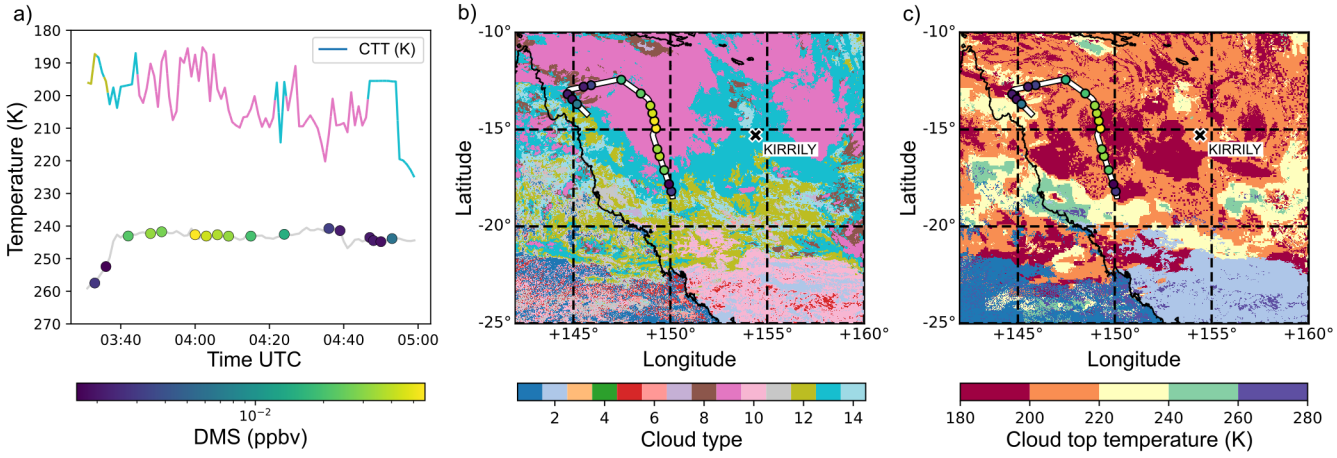

Figure 4. Convective outflow observed during RF7 on January 21 2024. a) Time series of cloud-top temperature (CTT) colour-coded with the cloud type (CT) together with the DMS mixing ratios measured along the flight track. b) Flight track and DMS mixing ratios overlaid on the CT map. c) Flight track and DMS mixing ratios overlaid on the CTT map. CT and CTT data correspond to 05 UTC on January 21 2024. Cloud type legend: 1 = cloud free land; 2 = cloud free sea; 3 = snow over-land; 4 = sea ice; 5 = very low clouds; 6 = low clouds; 7 = mid level clouds; 8 = high opaque clouds; 9 = very high opaque clouds; 10 = fractional clouds; 11 = high semitransparent thin clouds; 12 = high semitransparent moderately thick clouds; 13 = high semitransparent thick clouds; 14 = high semitransparent clouds above low or medium clouds. Colours 1 and 2 of the CT map have been adopted to represent cloud-free land and sea of the CTT map. The position of tropical cyclone Kirrily, denoted by the black cross, was reproduced with permission from the Bureau of Meteorology, ©Commonwealth of Australia.

The first event was recorded during RF7 on 21 January 2024 (Figure 4). While flying northward, HALO penetrated the upper-level (13–16 km) anvil that constituted the outflow cloud shield of a tropical depression, which intensified into Tropical Cyclone Kirrily over the following days. During the outflow passage, we measured elevated DMS mixing ratios, with a maximum of 56 pptv and decreasing quasi-exponentially across a swath of roughly 500 km until reaching the LOD. The highest DMS values were encountered within a very high, optically thick cloud deck, indicating that the aircraft was in close proximity to the convective core. Because the inflow region of the system was not sampled, we estimated the fraction of boundary layer DMS that reached the outflow by using the interquartile range of DMS mixing ratios observed below 1 km throughout the campaign (65–115 pptv) as bounding source values. This approach yields a concentration retention fraction of 49%–86% for boundary layer DMS lofted to the upper tropospheric outflow of a tropical depression.

The second event occurred during RF10 on 27–28 January 2024 as HALO flew from the Coral Sea towards the Indo-Pacific Warm Pool region (Figure 5). This area is characterised by extraordinarily low ozone concentrations in the upper troposphere, a consequence of non-electrified convection (Nussbaumer et al., 2025). The resulting scarcity of hydroxyl radicals prolongs the atmospheric lifetime of reactive trace gases such as DMS in this region (Kley et al., 1996; Rex et al., 2014). Between 22:00 and 22:30 UTC the aircraft traversed a small convective system and measured elevated DMS, reaching a maximum of 7.5 pptv. After remaining above a cloud deck, HALO entered the cloud field of a mesoscale convective system at 23:15 UTC. Within

https://doi.org/10.5194/egusphere-2026-5595
Preprint. Discussion started: 22 September 2026

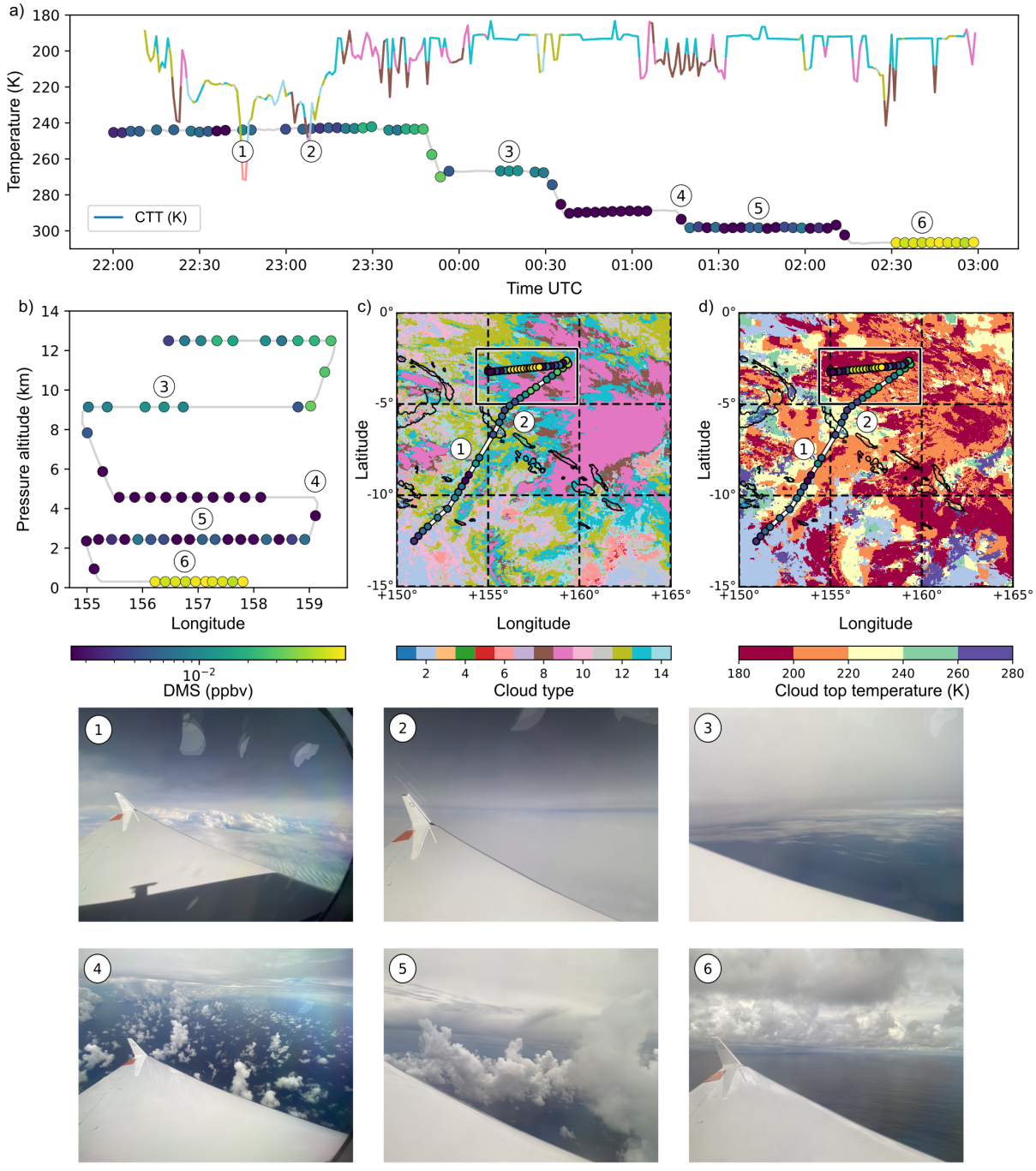

Figure 5. Convective outflow observed during RF10 on January 27–28 2024. a), c), d) analogue to Figure 4; CT and CTT data correspond to 01 UTC on January 28 2024. b) Longitude-altitude cross section of DMS mixing ratios through the convective system; the area shown corresponds to the box indicated in panels c)–d). Photographs 1-6 illustrate the observed cloud layers along the profile.

https://doi.org/10.5194/egusphere-2026-5595
Preprint. Discussion started: 22 September 2026

this system DMS mixing ratios rose to as high as 33 pptv at altitudes of 9.5–12.5 km and persisted over a horizontal distance of roughly 300 km. The vertical structure of the system was sampled with five stacked flight legs at different altitudes (Figure 5 b). Below the anvil, several small cumulus "towers" were observed near 2.4 km altitude (pictures 4–6 in Figure 5), which exhibited slightly elevated DMS mixing ratios of around 7 pptv. DMS mixing ratios during the lowest flight level (0.3 km), which we consider representative of the boundary layer inflow, ranged from 54 to 92 pptv, implying a concentration retention fraction of 36–61% for the lofting of DMS into the upper tropospheric outflow.

These concentration retention fractions are approximate estimates of the DMS that can be advected into the upper-tropospheric outflow of deep convective systems. Because the age of the studied outflows is uncertain and they may already have undergone some loss prior to being sampled, the values reported here should be interpreted as lower bounds on the true values.

The efficient vertical transport of DMS from the marine boundary layer to the upper troposphere may have ramifications for sulfur chemistry both aloft in the troposphere and even in the stratosphere. In the upper troposphere, DMS serves as a precursor for H_2SO_4 and sulfate aerosol formation via oxidation to SO_2 and MSA. To date, only a limited number of studies have examined DMS chemistry at these altitudes and associated temperatures and pressures, the majority of investigations having focused on the marine boundary layer (e.g., Barnes et al., 2006; Hoffmann et al., 2016; Korhonen et al., 2008; Quinn and Bates, 2011; Sanchez et al., 2018). The present results therefore motivate dedicated chamber experiments and modelling efforts that address DMS chemistry under cold and dry upper tropospheric conditions. Moreover, because troposphere-stratosphere exchange is exceptionally efficient in the tropical western Pacific (Fueglistaler et al., 2004; Bonazzola and Haynes, 2004), deep convective transport of DMS and its reaction products in this region could provide a pathway for its injection into the stratosphere, where they can persist for long periods and contribute to the Junge layer of stratospheric aerosol, as previously proposed by Marandino et al. (2013).

3.1.3 Diel variations

Diel cycles of DMS mixing ratios in the planetary boundary layer have been documented for both environments. Over the Amazon rainforest, DMS exhibits a modest midday maximum that coincides with a peak in photosynthetic available light (PAR) and temperature (Jardine et al., 2015). In contrast, marine boundary layer DMS concentrations increase overnight and display a midday minimum, reflecting the strongest photochemical loss during daylight hours (Andreae and Raemdonck, 1983; Nowak et al., 2001; Jackson et al., 2020).

Here we present, for the first time, the diel distribution of DMS mixing ratios throughout the entire tropospheric column for the CAFE-Brazil and CAFE-Pacific campaigns (Figure 6). In both regions, the DMS vertical distribution follows the diel pattern of convective activity (Yang and Slingo, 2001). Over the rainforest, larger DMS fluxes are lofted into the free, and occasionally upper, troposphere in the afternoon, consistent with the afternoon peak in convection (Machado et al., 2004). Over the Pacific Ocean, upper tropospheric DMS concentrations peak in the morning, matching the typical late morning maximum in marine convection (Pope et al., 2008).

However, these diel profiles must be interpreted with caution. The dataset, especially in the upper troposphere, does not represent background conditions because the flights were deliberately targeted toward areas of intense convective activity.

https://doi.org/10.5194/egusphere-2026-5595
Preprint. Discussion started: 22 September 2026

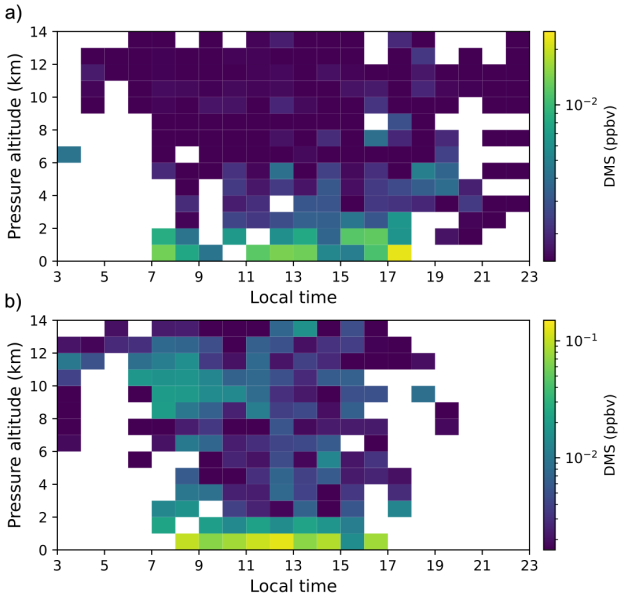

Figure 6. Diel variation of DMS volume mixing ratios. a) CAFE-Brazil data, local time corresponds to AMT (UTC-0400). b) CAFE-Pacific over-ocean data, local time corresponds to AEST (UTC+1000). Both data sets are displayed as gridded mean values within 1 hr×1 km grid cells.

3.2 Global model simulations

In this section, we compare the observational data with simulations of the state-of-the-art atmospheric chemistry model EMAC, with special emphasis on the representation of DMS sources and vertical transport.

3.2.1 Marine DMS emissions

The model results from the L11, W20 and H22 simulations (Table 1) were used to evaluate the agreement between the simulated DMS fields with our observations in the boundary layer (<0.5 km). The corresponding correlations and the spatial distribution of the model-to-observation ratios are shown in Figure 7, and for each correlation we report the coefficient of determination (R^2), the median model-to-observation ratio (M/O), and the percentage of points that lie within a factor of 2 of the observations (PF2).

In the boundary layer, the L11 simulation overestimates DMS by an average of 43% relative to our measurements and shows essentially no correlation with the observations (Figure 7 a). The bias is especially large over the Bismarck Sea and north of Papua New Guinea (Figure 7 d). In contrast, the W20 simulation underestimates DMS by about 34% on average and explains less of the observed variability ($R^2 = 0.141$). The H22 simulation on average gives a close match with the measured values ($M/O \approx 1$) and reproduces the observed variability best among the tested climatologies ($R^2 = 0.228$). These results demonstrate that the updates from Lana et al. (2011) to Hulswar et al. (2022) substantially improve the representation of seawater DMS,

https://doi.org/10.5194/egusphere-2026-5595
Preprint. Discussion started: 22 September 2026

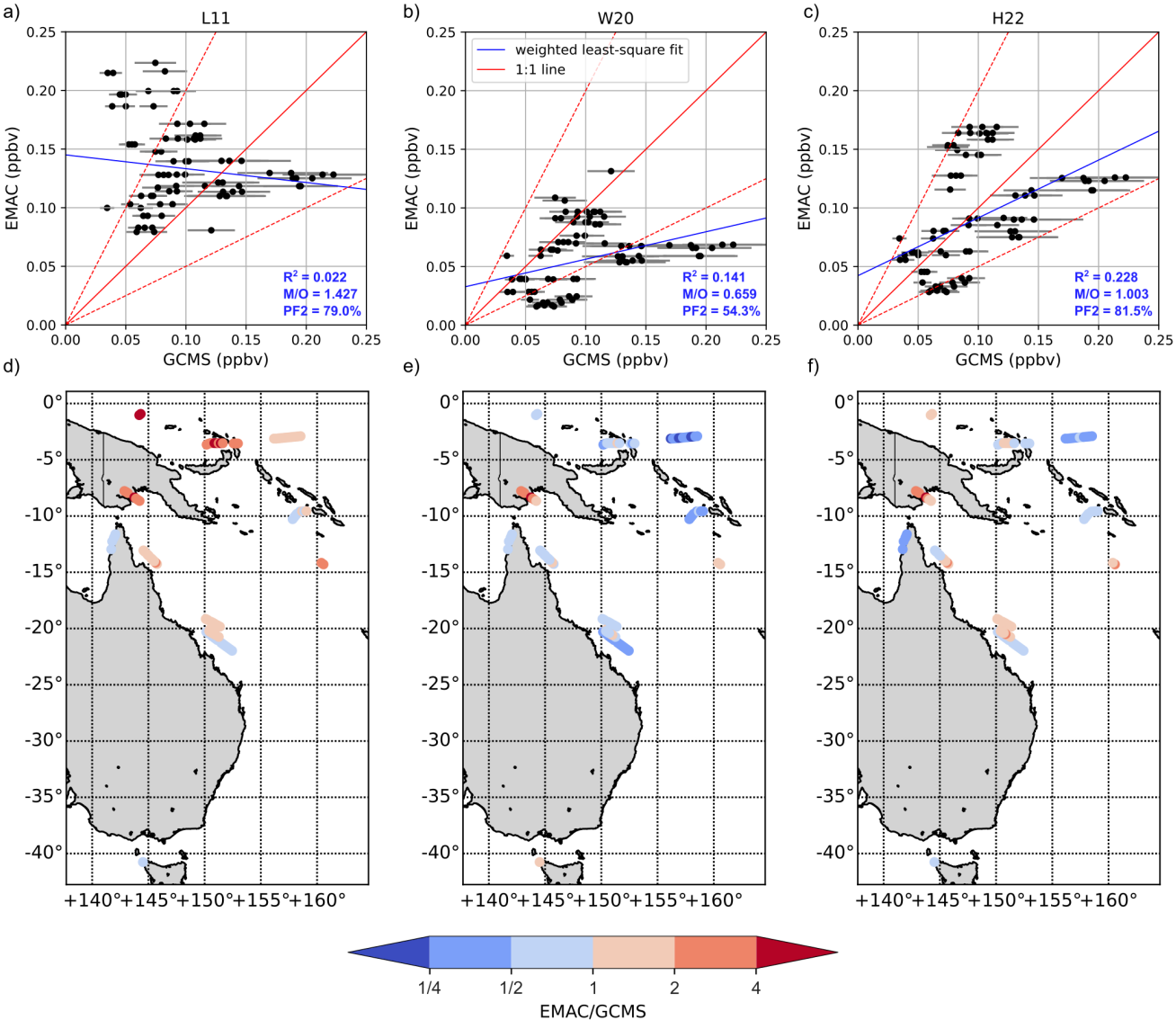

Figure 7. Comparison of GC-MS DMS measurements with EMAC simulations for the marine boundary layer (<0.5 km). a)–c) Scatter plots of observed mixing ratios versus simulated mixing ratios for three emission climatologies: a) L11, b) W20, and c) H22. Data from RF22 was excluded because the sampled airmasses were strongly influenced by terrestrial emissions. The blue line in each panel is a weighted least squares fit, with weights equal to the inverse of the squared relative measurement uncertainties (error bars in grey). The coefficient of determination (R^2), the median model-to-observation ratio (M/O), and the percentage of points within a factor of 2 of the observation (PF2) are indicated. d)–f) Spatial maps of the model-to-observation ratio for the same climatologies.

https://doi.org/10.5194/egusphere-2026-5595
Preprint. Discussion started: 22 September 2026

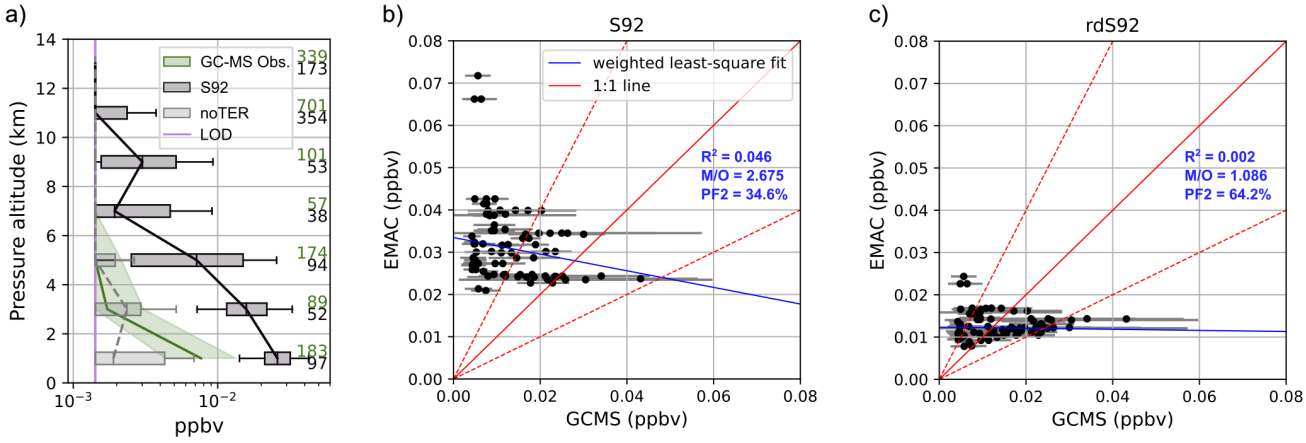

Figure 8. Comparison of observed and simulated DMS mixing ratios for CAFE-Brazil. a) Vertical distribution, GC-MS observation in green, the simulation using the S92 climatology in black, and the noTER simulation with marine emissions only in grey. Values below the GC-MS LOD (illustrated as a purple line) have been replaced with the LOD in both observed and simulated DMS data. b)–c) Scatter plots of observed versus simulated mixing ratios below 1 km, in b) for the S92, and in c) for the rdS92 simulation. Same as Figure 7 a–c.

making the latter the most suitable choice for the season and region examined. Consequently, we adopted the Hulswar et al. (2022) climatology for marine DMS emissions in our CAFE-Brazil simulations.

3.2.2 Terrestrial DMS emissions

For the CAFE-Brazil campaign, we ran the S92 simulation using the sole terrestrial DMS inventory available in the literature by Spiro et al. (1992). However, the monthly fixed climatological emissions do not reproduce any of the observed variability (Figure 8 b) and overestimate boundary layer DMS (<1 km) by roughly a factor of 2.7, which propagates into an excess throughout the entire tropospheric column (Figure 8 a). To quantify the contribution of terrestrial emissions to the total DMS, we performed the noTER simulation in which terrestrial DMS emissions were switched off, allowing only long-range-transported marine DMS to enter the central Amazonian domain. In this "marine-only" simulation, the simulated mixing ratios below 2 km are substantially lower than our observations, indicating that the bulk of DMS measured above the central Amazon originates from terrestrial sources. Scaling the terrestrial Spiro et al. (1992) emissions by a factor of 0.39 (the inverse of M/O = 2.675 for S92) brings M/O close to unity but does not improve the coefficient of determination (rdS92 simulation, Figure 8 c), indicating that a simple linear scaling cannot rectify the structural deficiencies of the inventory. These results demonstrate the need for a refined terrestrial DMS emission parametrisation, and the present observations can provide a benchmark for developing such a scheme.

https://doi.org/10.5194/egusphere-2026-5595
Preprint. Discussion started: 22 September 2026

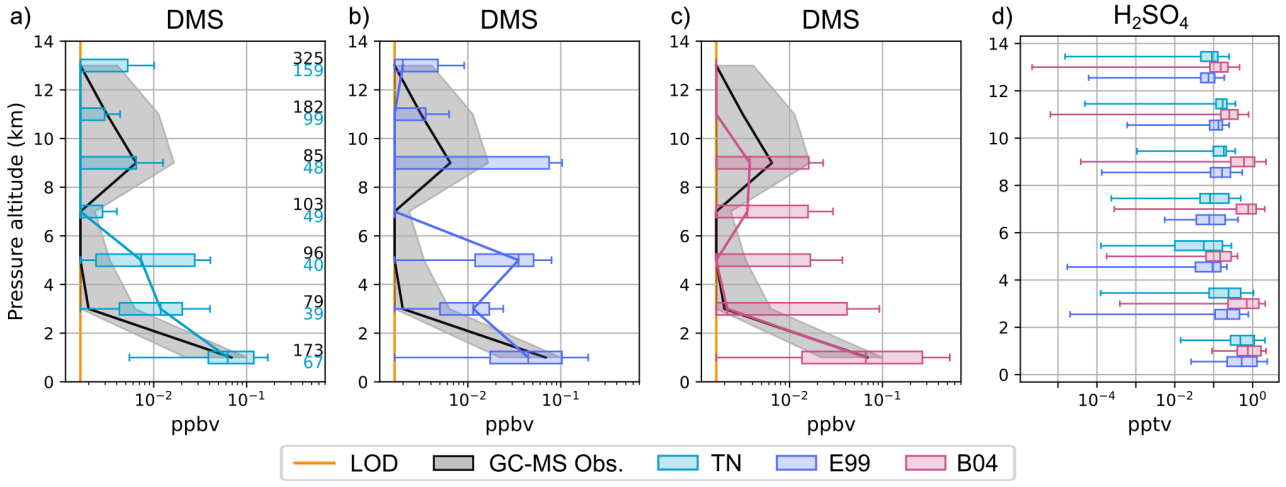

Figure 9. Vertical distribution of DMS and sulfuric acid (H_2SO_4) from EMAC simulations using different convection parametrisations compared to the GC-MS over-ocean DMS observations: a) Tiedke-Nordeng scheme (TN), b) Emanuel and Živković-Rothman scheme (E99), c) ECMWF scheme (B04). The solid lines correspond to the median in each altitude bin; the grey area indicates the 25th–75th percentile range of the observations. Values below the LOD were set to the LOD for both observed and simulated DMS data to facilitate direct comparison. d) Simulated H_2SO_4 for all three convection schemes. Data are binned in 2 km intervals, and the number of observations (black) and respective simulations (blue) in each altitude bin are given on the right side of panel a).

3.2.3 Vertical profile

To evaluate how well EMAC reproduces the observed convection during the CAFE-Pacific campaign, we compare the measured and simulated vertical distributions of DMS mixing ratios across the TN, B04 and E99 simulations (Figure 9 a–c). The results from both the TN and E99 simulations exhibit a difference to the observations in the mid troposphere (2–6 km), with modelled mixing ratios more than one magnitude higher than the observations. This could be caused by an overestimation of mid-level detrainment in these schemes. In contrast, the B04 scheme does not generate such a feature; however, it places the main convective outflow between 6 and 10 km, which is roughly 2 km lower than observed. Figure 9 d illustrates how the choice of convection scheme affects H_2SO_4, a secondary oxidation product of DMS and other reduced sulfur species. In the mid-troposphere, the simulated H_2SO_4 concentrations differ by up to an order of magnitude among the three schemes, demonstrating that convection parametrisation also strongly influences secondary sulfur chemistry.

In the upper troposphere (9–14 km), the median DMS mixing ratios produced by all three simulations are significantly lower than the aircraft measurements. This difference is partly due to the coarse horizontal resolution of EMAC, which does not allow the simulation of the small-scale convective features. Figure 10 compares the modelled upper-tropospheric DMS fields from the TN simulation with the observations for the two case studies presented in Figures 4 and 5. The figure shows that the model does generate DMS updrafts of comparable magnitude to those observed; however, the simulated updrafts are displaced slightly relative to the flight track. Consequently, a direct, point-by-point comparison between model output sampled along the

https://doi.org/10.5194/egusphere-2026-5595
Preprint. Discussion started: 22 September 2026

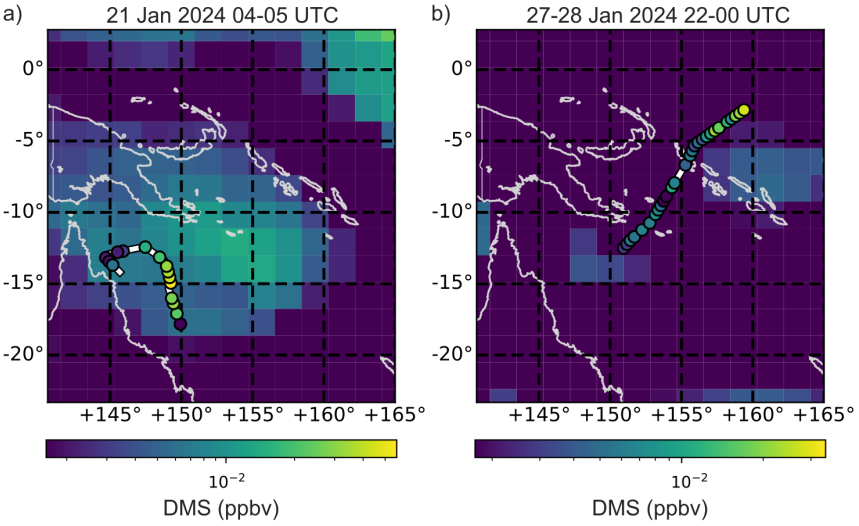

Figure 10. Upper tropospheric DMS mixing ratios (12–14 km) measured during CAFE Pacific plotted on top of the corresponding gridded maximum values from the TN simulations for the same time period and altitude range. a) Flight segment of RF7 (see also Figure 4); b) flight segment of RF10 (see also Figure 5). Measurements below the LOD have been replaced with the LOD. Simulations are binned into 1.875°x1.875° intervals. Please note that both panels have their own colour bars indicated below.

flight path and the measurements is ambiguous. Nonetheless, the results indicate that the TN and E99 simulations generally reproduce the observed mixing ratio magnitudes, albeit sometimes at different locations, whereas the B04 simulation markedly underestimates DMS transport to the upper troposphere.

Overall, the TN simulation yields the closest agreement with the observations, although notable differences persist in the mid-troposphere. Our sensitivity analysis shows that the choice of convection parametrisation controls not only the vertical distribution of DMS but also the concentrations of its oxidation products that are generated in the model. Consequently, an appropriate representation of deep convection is essential for global-scale studies of upper-tropospheric sulfur chemistry and for assessing its potential climate impacts.

4 Conclusions

In this study, we present airborne, in situ measurements of DMS from the CAFE-Brazil and CAFE-Pacific campaigns that span the tropospheric column from 0.3 km to 14 km over the Amazon rainforest and the eastern Indo Pacific Ocean. The boundary layer mixing ratios and the vertical profile of DMS in the lower troposphere are consistent with earlier gas chromatographic observations above tropical rainforest (Andreae and Andreae, 1988; Andreae et al., 1990). In the upper troposphere, DMS was generally below the LOD in deep convectively up-drafted air masses above the Amazon Basin. The boundary layer data confirm

https://doi.org/10.5194/egusphere-2026-5595
Preprint. Discussion started: 22 September 2026

the existence of a terrestrial source and the previously reported east-west gradient, which may be linked to a geoecological gradient rather than to transport of marine DMS.

The vertical profile of DMS in the lower and mid-troposphere over the eastern Indo Pacific Ocean agrees well with previous measurements, for example, those measured aboard the DC-8 during the PEM Tropics-B campaign. In the upper troposphere (9-14 km), we frequently observed elevated DMS in deep convective outflows, reaching up to 56 pptv, a phenomenon that has been previously observed only rarely (Thornton et al., 1997; Marandino et al., 2013). These observations highlight the need for further research on the fate of lofted DMS and its role in new particle formation at low temperatures and pressures typical of the upper troposphere and stratosphere.

For the season and region sampled during the CAFE-Pacific campaign, the model simulation using the marine emission inventory of Hulswar et al. (2022) provides the most accurate simulated DMS mixing ratios, although further refinements are necessary. Among the convection parametrisations tested, the EMAC default Tiedtke scheme with Nordeng closure (Tiedtke, 1989; Nordeng, 1994) yields the closest agreement with the observed vertical distribution, although it overestimates mixing ratios in the mid-troposphere. In the upper troposphere, the simulated lofted DMS mixing ratios match the observed magnitudes, but the model often predicts the updrafts slightly displaced from the aircraft trajectory.

Comparison of EMAC simulations using the terrestrial DMS inventory of Spiro et al. (1992) with the CAFE-Brazil observations shows that simulations using this climatology overestimate DMS mixing ratios above the Amazon rainforest by roughly a factor of three. Although the oceanic source dominates the global DMS budget and terrestrial emissions contribute only a minor fraction, such an overestimate can produce a regional excess of DMS throughout the troposphere, with potential consequences for regional sulfur chemistry. Our work, therefore, motivates the improvement of terrestrial DMS emissions in numerical models. Future work should focus on improving the understanding of terrestrial, particularly plant-derived, DMS sources and obtaining additional atmospheric observations in continental, forested regions.

Data availability. The observational datasets for CAFE-Brazil and CAFE-Pacific will be uploaded to the HALO database (https://halo-db.pa.op.dlr.de/) upon acceptance of the manuscript. The PEM Tropics-B data are available through the NASA Langley Atmospheric Science Data Center Distributed Active Archive Center (https://doi.org/10.5067/ASDC/SUBORBITAL/PEM-TROPICS-B/MERGE_DATA_1) (GTE Project Office et al., 2025). The simulation data are available on request.

Appendix A: CFC correction

A common strategy for reducing systematic and random errors in quantitative GC-MS analysis is the use of an internal standard, an added compound (absent from the original sample) at a known concentration, to monitor sampling biases and detector sensitivity drift. Isotopically labelled molecules (e.g., ^{2}H- or ^{13}C-labeled) are frequently employed. For instance, $^{2}H_8$-toluene was used as an internal standard for ambient VOC measurements (Demeestere et al., 2008). We did not purposely introduce such an internal standard to our samples. Instead, we exploited the quasi uniform presence of long-lived CFCs in the tropo-

https://doi.org/10.5194/egusphere-2026-5595
Preprint. Discussion started: 22 September 2026

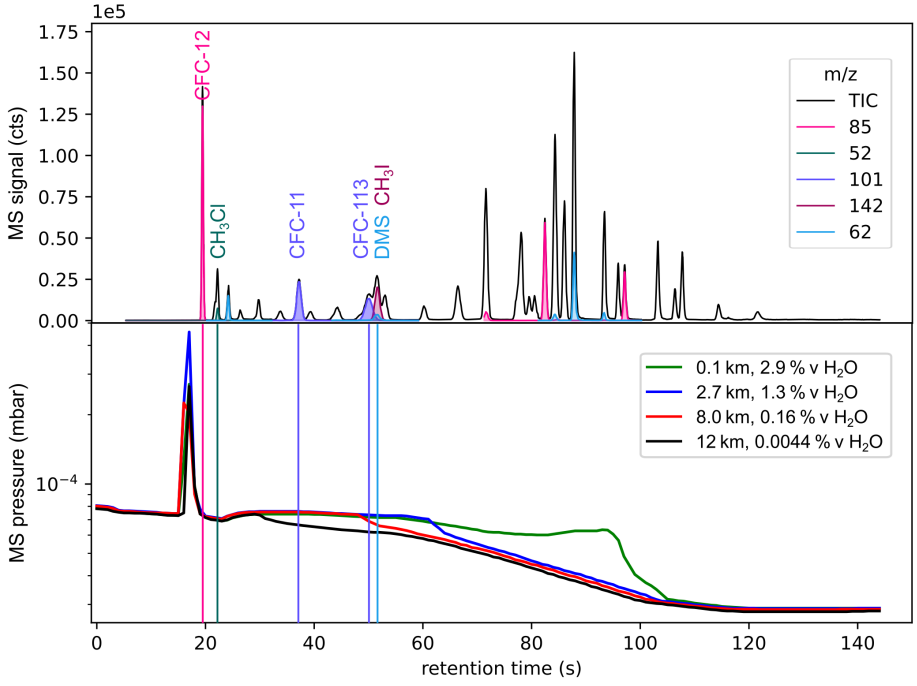

Figure A1. Upper panel: Representative calibration chromatogram obtained with the Fast GC MS system. Lower panel: Corresponding MS pressure recorded throughout the chromatogram at different altitude and humidity conditions during RF7 of CAFE-Brazil.

sphere and used them as an internal standard because their mixing ratios are spatially homogeneous. By normalising the VOC signals to the nearby CFC peaks, we corrected for variations in instrument sensitivity caused by CO_2 and humidity.

The typical variation of MS pressure during a chromatographic run is shown in Figure A1. The sharp peak at the beginning (~ 16–17 s) corresponds to the elution of CO_2, which is trapped in the -160 °C enrichment trap together with all other VOCs. The subsequent, broader feature (~ 25–105 s) is caused by water vapour. Both CO_2 and water are present at significantly higher concentrations than VOCs in the atmosphere. Although most of the sample's water was expected to be removed by the -10 °C cold trap before enrichment, our results indicate that a substantial fraction of water vapour nevertheless survived this stage and entered the GC-MS system. The magnitude of the water feature was highly variable throughout a RF, closely linked to the flight altitude and the corresponding ambient humidity. Conversely, the MS pressure can be used as a proxy for the water abundance in the MS at a given retention time.

CFCs are highly volatile, chemically inert substances that were used industrially (e.g., as refrigerants) from the 1930s until their ban under the Montreal Protocol in the late 1980s because of their strong ozone-depleting potential (Kim et al., 2011). Their long atmospheric lifetimes (CFC-11: 43 yr; CFC-12: 88 yr; CFC-113: 72 yr) exceed the timescales of tropospheric mixing, resulting in uniform background mixing ratios throughout the troposphere. These background mixing ratios are continuously monitored by a global network of long-term measurements, such as the Advanced Global Atmospheric Gases

https://doi.org/10.5194/egusphere-2026-5595
Preprint. Discussion started: 22 September 2026

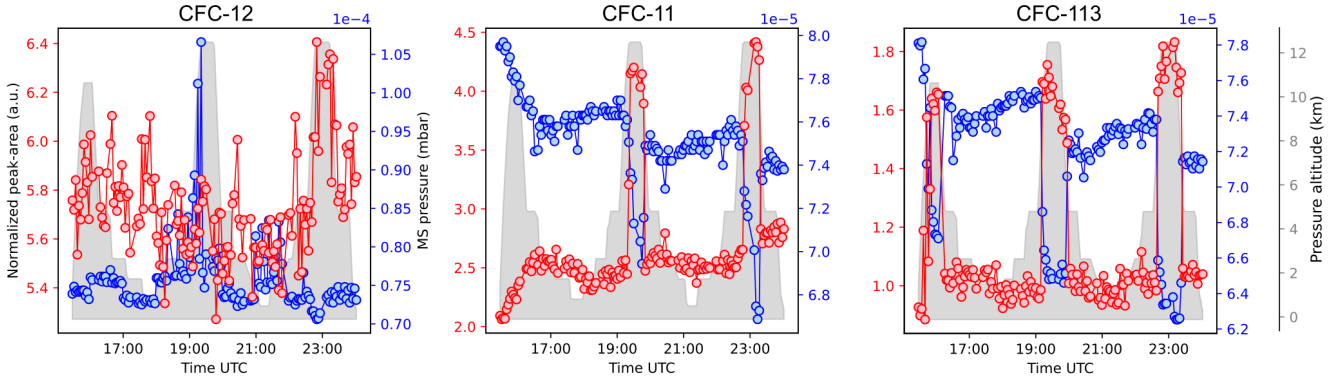

Figure A2. Normalised peak areas of CFC-12, CFC-11, and CFC-113 from ambient samples measured during RF7 of CAFE-Brazil are shown in red (left y-axis). The right y-axis shows the pressure inside the MS at the approximate retention time of each compound, plotted in blue. Y-axis labels are the same for every panel, but are only shown in the first one for clarity. The grey area indicates the flight altitude, with the corresponding y-axis on the right side of the figure.

Experiment (AGAGE) (Prinn et al., 2018) and the NOAA flask samples (Montzka et al., 1999), making CFCs excellent tracers for assessing instrument sensitivity. CFC-12 (ret. time = 19.8 s, $m/z = 85$), CFC-11 (ret. time = 36.3 s, $m/z = 101$), and CFC-113 (ret. time = 47.7 s, $m/z = 101$) were included in our method. For their background mixing ratios, we adopted the following reference values:

- CFC-12: monthly averages of the high-resolution dataset by Prinn et al. (2025).
- CFC-113: averages derived from flask measurements by Stephen A. Montzka and Isaac Vimont (downloaded from https://gml.noaa.gov/aftp/data/hats/cfcs/cfc113/flasks/GCMS/CFC113_GCMS_flask.txt on 23 August 2026).

Both datasets were obtained at the Kennaook/Cape Grim Baseline Air Pollution Station (Tasmania, Australia), which provides a well-characterised, clean air baseline for the Southern Hemisphere (Fraser et al., 2020).

The time series of CFC-11, CFC-12, and CFC-113 recorded during the RFs (red curves in Figure A2) show pronounced variability, with each compound displaying a distinct pattern. For CFC-11 and CFC-113, the variability is especially large: recorded peak areas at high altitude can be up to a factor of two higher than at lower altitudes. This behaviour follows the changes in MS pressure at the retention times of their peaks, suggesting that increased water vapour in the ion source reduces sensitivity. A higher abundance of ionised H_2O molecules creates a denser space-charge cloud within the ion source, which can perturb ion trajectories and prevent efficient transmission of analyte ions out of the source (Cowen et al., 1993).

In contrast, CFC-12 exhibits lower variability (~ 10%), which appears not correlated with MS pressure (Figure A2). A similar space-charge effect may still be present because the tail of the CO_2 peak overlaps the CFC-12 retention window. The lack of an observable relationship could be partly due to the MS pressure being recorded at only 1 Hz, which is insufficient to resolve the rapidly changing pressure associated with the relatively narrow CO_2 peak. Moreover, the tropospheric variability of CO_2 concentrations is modest. For example, a CO_2 variability of up to 10% has been reported in the boundary layer above a tropical

https://doi.org/10.5194/egusphere-2026-5595
Preprint. Discussion started: 22 September 2026

rainforest in Suriname (Williams et al., 2001), while variability above the boundary layer is expected to be considerably smaller. This magnitude is consistent with the observed CFC-12 variability.

Finally, additional factors that influence all compounds equally should be considered, such as the water dilution effect, which is explained in detail elsewhere (Harazono et al., 2015), and other instrumental effects like electrical drift of the MS.

To correct for these various influences on instrument sensitivity, we normalised each analyte peak to a nearby CFC peak. This approach rests on three assumptions:

1. The prevailing conditions in the MS at a given retention time affect the sensitivity to all compounds in the same manner.
2. Peaks that are close in retention time to each other (approx. 2 s apart from each other) experience the same sensitivity conditions.
3. Ambient CFC mixing ratios are vertically and spatially homogeneous throughout the troposphere (Zeng et al., 2022) and can be represented by the well-established background values reported in the literature.

Under these premises, the CFC peaks provide an internal reference that corrects for altitude-, humidity-, and instrument-related sensitivity variations affecting nearby VOC signals. Only VOCs whose retention times lie close to a CFC peak can be corrected with this method. In the present dataset, these are CH_3Cl, which was corrected with the CFC-12 signal, and DMS and CH_3I, which were corrected with CFC-113.

The first step of the correction was to flag any sample in which the MS pressure at the retention time of the CFC and the analyte differed by more than 2%. Such samples violate the second assumption (that both peaks experience comparable conditions) and were excluded from further analysis. For DMS, this criterion removed 6.5% of the CAFE-Brazil in-flight samples and 6.8% of the CAFE-Pacific samples, most of which were recorded during ascent or descent.

For the remaining samples, the background contribution was subtracted, after which correction factors for the calibration samples were derived. This was done by forcing the CFC calibration points onto a straight line through the origin and an arbitrarily chosen reference peak area at the corresponding background mixing ratio (denoted as cyan stars in Figure A3 b,f). In the next step, correction factors were applied to the areas of the corresponding VOCs for each calibration sample. The final calibration parameters for CH_3Cl, DMS, and CH_3I were obtained as the mean slope of the corrected in-flight calibration points (blue line in Figure A3).

As shown in Figure A3, the CFC correction significantly reduces the variability of the calibration points for all three analytes. For DMS, however, the corrected in-flight calibration points remain systematically lower than the ground-based calibrations. We attribute this discrepancy to an additional humidity effect in our inlet. Under more humid conditions, DMS may adsorb less efficiently to the stainless steel inlet lines, leading to enhanced transmission. This hypothesis is supported by the observation that, after correcting for the water-induced MS sensitivity loss, the DMS instrument response exhibits a linear relationship with MS pressure (see Figure A4), which is a proxy for the water vapour level in the instrument. Because the difference between high and low humidity conditions exceeds a factor of two for DMS, we used this linear relationship to correct the DMS signal.

Between the CAFE-Brazil and CAFE-Pacific campaigns, the platinum pellets in the Zero Air-Generator were replaced during routine maintenance, introducing an additional source of humidity into the calibration system. Consequently, only a few

https://doi.org/10.5194/egusphere-2026-5595
Preprint. Discussion started: 22 September 2026

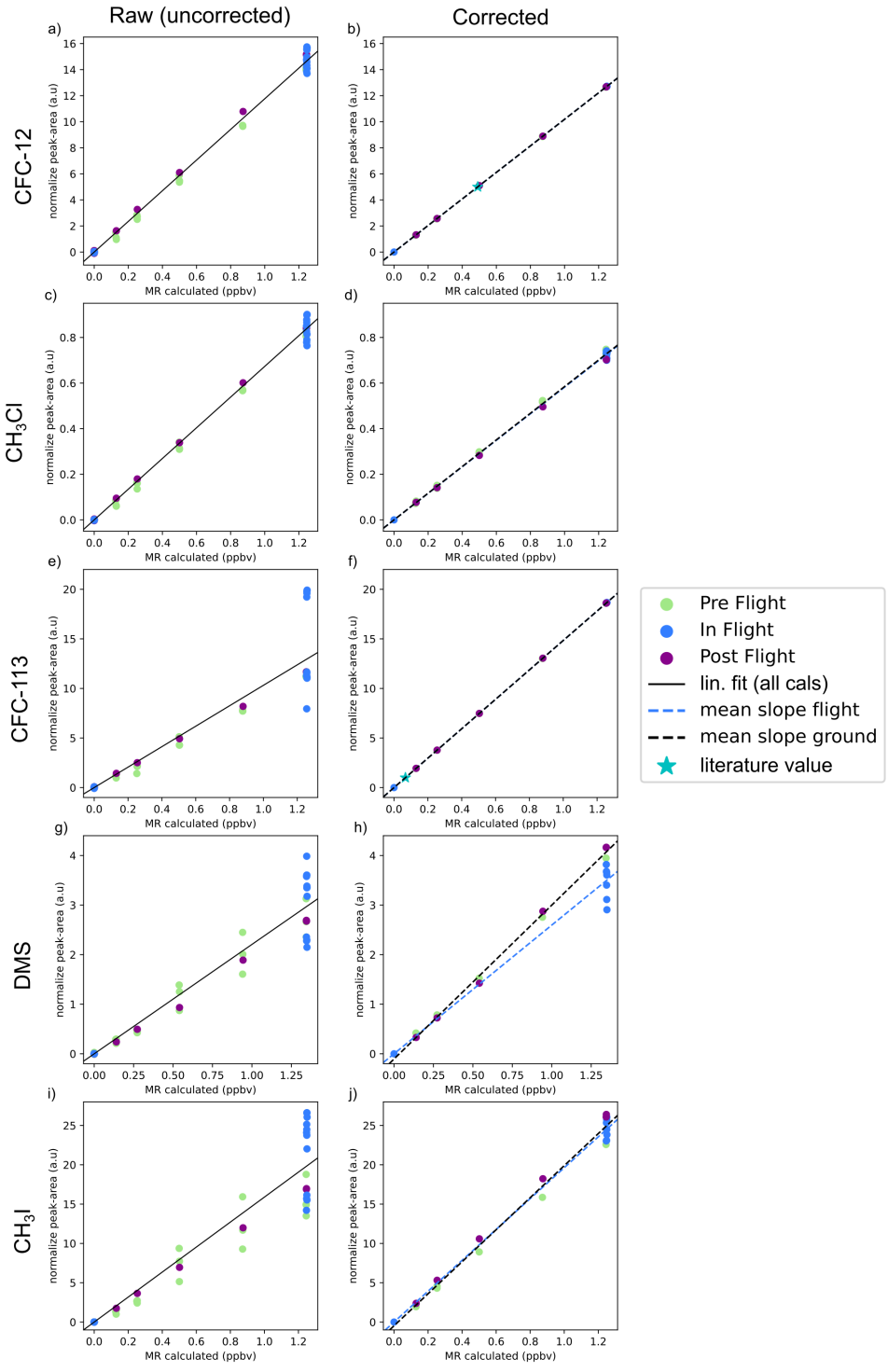

Figure A3. Calibration samples from RF7 during CAFE-Brazil before and after applying the CFC correction.

https://doi.org/10.5194/egusphere-2026-5595
Preprint. Discussion started: 22 September 2026

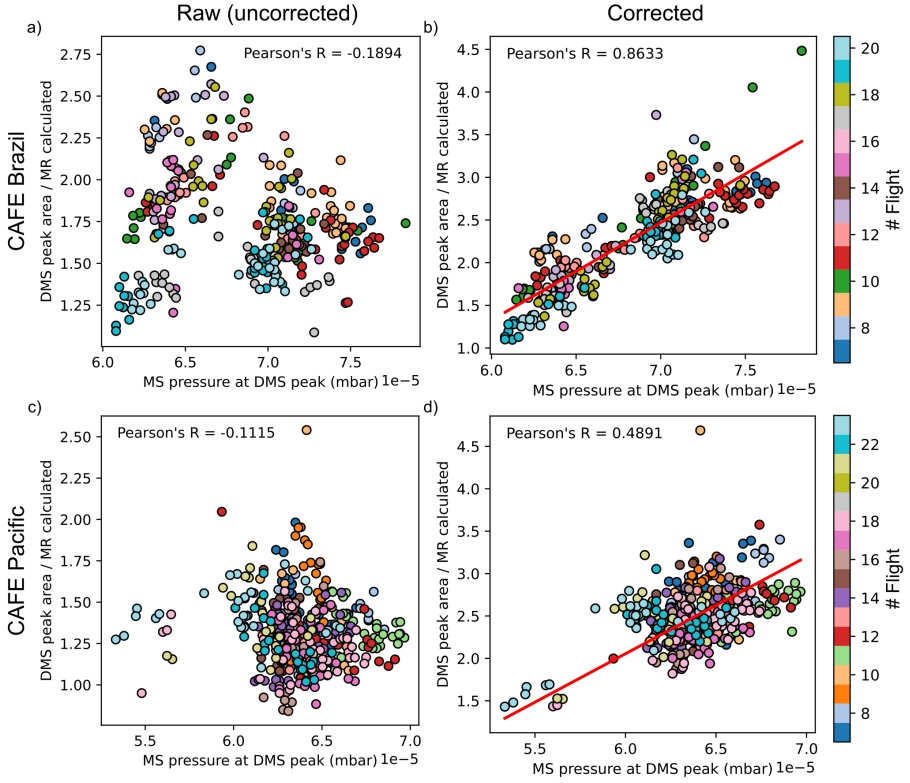

Figure A4. Correlation between the instrument response (peak area divided by the injected mixing ratio) and the mass spectrometer pressure at the DMS retention time, shown before (a,c) and after (b,d) applying the CFC correction across all calibration points of the respective campaign (ground and in-flight). The red line denotes the calibration parametrisation: a linear regression for CAFE-Brazil. Because only a few dry calibration points were available for CAFE-Pacific, the slope from the CAFE-Brazil calibrations was retained, and the intercept was adjusted to best match the CAFE-Pacific data. See text for more details.

dry calibrations at high altitude were obtained during the later flights (RF18 onward) of CAFE-Pacific. Since the calibration points for CAFE-Brazil are more evenly distributed between wet and dry conditions, we retained the slope derived from the CAFE-Brazil calibrations for both campaigns and adjusted only the y-intercept for CAFE-Pacific to achieve the best fit. This adjustment was necessary because the foreline pump of the mass spectrometer was replaced between the campaigns, resulting in generally slightly lower MS pressure during CAFE-Pacific.

The additional uncertainty associated with the assumption of uniform CFC background mixing ratios throughout the troposphere was conservatively set to 5% of the literature CFC mixing ratios. This value encompasses the 0.12% Kennaook/Cape Grim instrument precision (Miller et al., 2008), the approx. 2% variability of CFC surface mixing ratios observed over the two-month campaign periods across nine AGAGE stations around the globe, and an extra margin to account for variability within the vertical tropospheric column. To account for the additional uncertainty of the humidity correction of DMS mixing

https://doi.org/10.5194/egusphere-2026-5595
Preprint. Discussion started: 22 September 2026

ratios, the least-square fit uncertainty was employed. All steps of the correction were considered in the error propagation and are therefore reflected in the total uncertainty reported above.

Appendix B: Reactions involving DMS in the MIM1 atmospheric chemistry mechanism

Table B1. Second order rate coefficients of reactions involving DMS in the MIM1 atmospheric chemistry mechanism. T refers to the temperature in K, while $[O_2]$ stands for the oxygen concentration in cm^{-3}.

Reaction	Rate coeff. (cm^3 s^{-1})	Reference
DMS + OH $\longrightarrow$ CH_3SO_2 + HCHO	$1.13 * 10^{-11} * e^{\frac{-253}{T}}$	Atkinson et al. (2004)
DMS + OH $\longrightarrow$ DMSO + HO_2	$\frac{1.0*10^{-39}*e^{\frac{5820}{T}}*[O_2]}{(1+5.0*10^{30}*e^{\frac{6280}{T}}*[O_2])}$	Atkinson et al. (2004)
DMS + NO_3 $\longrightarrow$ CH_3SO_2 + HNO_3 + HCHO - O_3	$1.9 * 10^{-13} * e^{\frac{520}{T}}$	Atkinson et al. (2004)
DMS + Cl $\longrightarrow$ CH_3SO_2 + HCl + HCHO	$3.3 * 10^{-10}$	Atkinson et al. (2004)
DMS + Br $\longrightarrow$ CH_3SO_2 + HBr + HCHO	$9.0 * 10^{-11} * e^{\frac{-2386}{T}}$	Jefferson et al. (1994)
DMS + BrO $\longrightarrow$ DMSO + Br	$4.4 * 10^{-13}$	Ingham et al. (1999)

Author contributions. BEK, JL, and JW designed the study. BEK conducted the measurements and processed the flight data, with contributions from JB and AG. MK and AM prepared the EMAC simulations, with supervision from AP. MH retrieved and processed the satellite data. BEK analysed and interpreted the data and wrote the manuscript with contributions from all co-authors.

Competing interests. At least one of the co-authors is a member of the editorial board of Atmospheric Chemistry and Physics.

Acknowledgements. This research has been funded by the Max Planck Society. The authors thank NASA's Ocean Color Earthdata OB.DAAC for providing Aqua-MODIS ocean Chlorophyll concentrations (OCI-Algorithm) used in Figure 3 (acquired November 11 2025). Himawari 8/9 satellite data was provided by the Australian Bureau of Meteorology and distributed via the NCI THREDDS Data Service. The PEM Tropics-B data used in this publication were obtained from Donald Blake (UC Irvine) as part of the Network for the Detection of Atmospheric Composition Change (NDACC) and are available through (https://ndacc.larc.nasa.gov/). The authors gratefully acknowledge the NOAA Air Resources Laboratory (ARL) for the provision of the HYSPLIT transport and dispersion model and/or READY website (https://www.ready.noaa.gov) used in this publication. AGAGE is supported principally by the National Aeronautics and Space Administration (USA) grants to the Massachusetts Institute of Technology and the Scripps Institution of Oceanography. The Kennaook/Cape Grim station is funded and managed by the Australian Bureau of Meteorology, with the AGAGE scientific program jointly managed with the Commonwealth Scientific and Industrial Research Organization (CSIRO). Support is also received from the Australian Department of Climate Change, Energy, the Environment and Water (DCCEEW), Refrigerant Reclaim Australia (RRA), and through the NASA Upper Atmospheric Research Program

https://doi.org/10.5194/egusphere-2026-5595
Preprint. Discussion started: 22 September 2026

award to MIT (80NSSC21K1369) with a sub-award to CSIRO for Kennaook/Cape Grim AGAGE activities. The authors acknowledge Stephen A. Montzka and Isaac Vimont for providing the NOAA flask data from Kennaook/Cape Grim. The model simulations have been performed at the German Climate Computing Centre (DKRZ) with support from the Max Planck Society. We gratefully acknowledge the staff from DLR-FX Oberpfaffenhofen for their support during the CAFE campaigns. Furthermore, we thank Philip Holzbeck for providing the photos taken during RF10 used in Figure 5.

https://doi.org/10.5194/egusphere-2026-5595
Preprint. Discussion started: 22 September 2026

References

Albu, M., Barnes, I., Becker, K. H., Patroescu-Klotz, I., Mocanu, R., and Benter, T.: Rate coefficients for the gas-phase reaction of OH radicals with dimethyl sulfide: temperature and O_2 partial pressure dependence, Phys. Chem. Chem. Phys., 8, 728–736, https://doi.org/10.1039/B512536G, 2006.

Andreae, M. O.: Ocean-atmosphere interactions in the global biogeochemical sulfur cycle, Marine Chemistry, 30, 1–29, https://doi.org/10.1016/0304-4203(90)90059-L, 1990.

Andreae, M. O. and Andreae, T. W.: The cycle of biogenic sulfur compounds over the Amazon Basin: 1. Dry season, Journal of Geophysical Research: Atmospheres, 93, 1487–1497, https://doi.org/10.1029/JD093iD02p01487, 1988.

Andreae, M. O. and Raemdonck, H.: Dimethyl Sulfide in the Surface Ocean and the Marine Atmosphere: A Global View, Science, 221, 744–747, https://doi.org/10.1126/science.221.4612.744, 1983.

Andreae, M. O., Berresheim, H., Bingemer, H., Jacob, D. J., Lewis, B. L., Li, S.-M., and Talbot, R. W.: The atmospheric sulfur cycle over the Amazon Basin: 2. Wet season, Journal of Geophysical Research: Atmospheres, 95, 16 813–16 824, https://doi.org/10.1029/JD095iD10p16813, _eprint: https://agupubs.onlinelibrary.wiley.com/doi/pdf/10.1029/JD095iD10p16813, 1990.

Atkinson, R., Baulch, D. L., Cox, R. A., Crowley, J. N., Hampson, R. F., Hynes, R. G., Jenkin, M. E., Rossi, M. J., and Troe, J.: Evaluated kinetic and photochemical data for atmospheric chemistry: Volume I - gas phase reactions of O_x, HO_x, NO_x and SO_x species, Atmospheric Chemistry and Physics, 4, 1461–1738, https://doi.org/10.5194/acp-4-1461-2004, 2004.

Ayers, G. P. and Gras, J. L.: Seasonal relationship between cloud condensation nuclei and aerosol methanesulphonate in marine air, Nature, 353, 834–835, https://doi.org/10.1038/353834a0, 1991.

Barnes, I., Hjorth, J., and Mihalopoulos, N.: Dimethyl Sulfide and Dimethyl Sulfoxide and Their Oxidation in the Atmosphere, Chemical Reviews, 106, 940–975, https://doi.org/10.1021/cr020529+, 2006.

Bechtold, P., Chaboureau, J.-P., Beljaars, A., Betts, A. K., Köhler, M., Miller, M., and Redelsperger, J.-L.: The simulation of the diurnal cycle of convective precipitation over land in a global model, Quarterly Journal of the Royal Meteorological Society, 130, 3119–3137, https://doi.org/10.1256/qj.03.103, _eprint: https://rmets.onlinelibrary.wiley.com/doi/pdf/10.1256/qj.03.103, 2004.

Bell, T. G., Porter, J. G., Wang, W.-L., Lawler, M. J., Boss, E., Behrenfeld, M. J., and Saltzman, E. S.: Predictability of Sea-water DMS During the North Atlantic Aerosol and Marine Ecosystem Study (NAAMES), Frontiers in Marine Science, 7, https://doi.org/10.3389/fmars.2020.596763, 2021.

Berresheim, H. and Vulcan, V. D.: Vertical distributions of COS, CS2, DMS and other sulfur compounds in a loblolly pine forest, Atmospheric Environment. Part A. General Topics, 26, 2031–2036, https://doi.org/10.1016/0960-1686(92)90087-2, 1992.

Bingemer, H. G., Andreae, M. O., Andreae, T. W., Artaxo, P., Helas, G., Jacob, D. J., Mihalopoulos, N., and Nguyen, B. C.: Sulfur gases and aerosols in and above the equatorial African rain forest, Journal of Geophysical Research: Atmospheres, 97, 6207–6217, https://doi.org/10.1029/91JD01112, _eprint: https://agupubs.onlinelibrary.wiley.com/doi/pdf/10.1029/91JD01112, 1992.

Bonazzola, M. and Haynes, P. H.: A trajectory-based study of the tropical tropopause region, Journal of Geophysical Research: Atmospheres, 109, https://doi.org/10.1029/2003JD004356, 2004.

Bourtsoukidis, E., Helleis, F., Tomsche, L., Fischer, H., Hofmann, R., Lelieveld, J., and Williams, J.: An aircraft gas chromatograph–mass spectrometer System for Organic Fast Identification Analysis (SOFIA): design, performance and a case study of Asian monsoon pollution outflow, Atmospheric Measurement Techniques, 10, 5089–5105, https://doi.org/10.5194/amt-10-5089-2017, 2017.

https://doi.org/10.5194/egusphere-2026-5595
Preprint. Discussion started: 22 September 2026

Brimblecombe, P. and Shooter, D.: Photo-oxidation of dimethylsulphide in aqueous solution, Marine Chemistry, 19, 343–353, https://doi.org/10.1016/0304-4203(86)90055-1, 1986.

Bureau Of Meteorology: Bureau of Meteorology Satellite Derived Products, https://doi.org/10.25914/5QRS-QB54, artwork Size: 75 TB Medium: netCDF Pages: 75 TB Version Number: 1, 2021.

Bureau Of Meteorology: Himawari 8/9 - Cloud Top Height and Temperature (CTTH), https://doi.org/10.25914/SRPZ-4Z64, 2024a.

Bureau Of Meteorology: Himawari 8/9 - Cloud Type (CT), https://doi.org/10.25914/C2VT-8N41, 2024b.

Carslaw, K. S., Lee, L. A., Reddington, C. L., Pringle, K. J., Rap, A., Forster, P. M., Mann, G. W., Spracklen, D. V., Woodhouse, M. T., Regayre, L. A., and Pierce, J. R.: Large contribution of natural aerosols to uncertainty in indirect forcing, Nature, 503, 67–71, https://doi.org/10.1038/nature12674, 2013.

Charlson, R., Langner, J., Rodhe, H., Leovy, C., and Warren, S.: Perturbation of the northern hemisphere radiative balance by backscattering from anthropogenic sulfate aerosols*, Tellus A: Dynamic Meteorology and Oceanography, 43, 152–163, https://doi.org/10.3402/tellusa.v43i4.11944, _eprint: https://doi.org/10.3402/tellusa.v43i4.11944, 1991.

Charlson, R. J., Lovelock, J. E., Andreae, M. O., and Warren, S. G.: Oceanic phytoplankton, atmospheric sulphur, cloud albedo and climate, Nature, 326, 655–661, https://doi.org/10.1038/326655a0, 1987.

Chen, Q., Sherwen, T., Evans, M., and Alexander, B.: DMS oxidation and sulfur aerosol formation in the marine troposphere: a focus on reactive halogen and multiphase chemistry, Atmospheric Chemistry and Physics, 18, 13 617–13 637, https://doi.org/10.5194/acp-18-13617-2018, 2018.

Chin, M. and Jacob, D. J.: Anthropogenic and natural contributions to tropospheric sulfate: A global model analysis, Journal of Geophysical Research: Atmospheres, 101, 18 691–18 699, https://doi.org/10.1029/96JD01222, _eprint: https://agupubs.onlinelibrary.wiley.com/doi/pdf/10.1029/96JD01222, 1996.

Colman, J. J., Swanson, A. L., Meinardi, S., Sive, B. C., Blake, D. R., and Rowland, F. S.: Description of the Analysis of a Wide Range of Volatile Organic Compounds in Whole Air Samples Collected during PEM-Tropics A and B, Analytical Chemistry, 73, 3723–3731, https://doi.org/10.1021/ac010027g, 2001.

Colomb, A., Gros, V., Alvain, S., Sarda-Esteve, R., Bonsang, B., Moulin, C., Klüpfel, T., and Williams, J.: Variation of atmospheric volatile organic compounds over the Southern Indian Ocean (30–49°S), Environmental Chemistry, 6, 70–82, https://doi.org/10.1071/EN08072, 2009.

Conley, S. A., Faloona, I., Miller, G. H., Lenschow, D. H., Blomquist, B., and Bandy, A.: Closing the dimethyl sulfide budget in the tropical marine boundary layer during the Pacific Atmospheric Sulfur Experiment, Atmospheric Chemistry and Physics, 9, 8745–8756, https://doi.org/10.5194/acp-9-8745-2009, 2009.

Cowen, M. C., Allison, W., and Batey, J. H.: Electron space charge effects in ion sources for residual gas analysis, Measurement Science and Technology, 4, 72–78, https://doi.org/10.1088/0957-0233/4/1/012, 1993.

Crutzen, P. J., Williams, J., Pöschl, U., Hoor, P., Fischer, H., Warneke, C., Holzinger, R., Hansel, A., Lindinger, W., Scheeren, B., and Lelieveld, J.: High spatial and temporal resolution measurements of primary organics and their oxidation products over the tropical forests of Surinam, Atmospheric Environment, 34, 1161–1165, https://doi.org/10.1016/S1352-2310(99)00482-3, 2000.

Curtius, J., Heinritzi, M., Beck, L. J., Pöhlker, M. L., Tripathi, N., Krumm, B. E., Holzbeck, P., Nussbaumer, C. M., Hernández Pardo, L., Klimach, T., Barmpounis, K., Andersen, S. T., Bardakov, R., Bohn, B., Cecchini, M. A., Chaboureau, J.-P., Dauhut, T., Dienhart, D., Dörich, R., Edtbauer, A., Giez, A., Hartmann, A., Holanda, B. A., Joppe, P., Kaiser, K., Keber, T., Klebach, H., Krüger, O. O., Kürten, A., Mallaun, C., Marno, D., Martinez, M., Monteiro, C., Nelson, C., Ort, L., Raj, S. S., Richter, S., Ringsdorf, A., Rocha, F., Simon, M.,

https://doi.org/10.5194/egusphere-2026-5595
Preprint. Discussion started: 22 September 2026

Sreekumar, S., Tsokankunku, A., Unfer, G. R., Valenti, I. D., Wang, N., Zahn, A., Zauner-Wieczorek, M., Albrecht, R. I., Andreae, M. O., Artaxo, P., Crowley, J. N., Fischer, H., Harder, H., Herdies, D. L., Machado, L. A. T., Pöhlker, C., Pöschl, U., Possner, A., Pozzer, A., Schneider, J., Williams, J., and Lelieveld, J.: Isoprene nitrates drive new particle formation in Amazon's upper troposphere, Nature, 636, 124–130, https://doi.org/10.1038/s41586-024-08192-4, 2024.

Demeestere, K., Dewulf, J., De Roo, K., De Wispelaere, P., and Van Langenhove, H.: Quality control in quantification of volatile organic compounds analysed by thermal desorption–gas chromatography–mass spectrometry, Journal of Chromatography A, 1186, 348–357, https://doi.org/10.1016/j.chroma.2007.11.036, 2008.

Droux, M.: Sulfur Assimilation and the Role of Sulfur in Plant Metabolism: A Survey, Photosynthesis Research, 79, 331–348, https://doi.org/10.1023/B:PRES.0000017196.95499.11, company: Springer Distributor: Springer Institution: Springer Label: Springer, 2004.

Emanuel, K. A. and Živković Rothman, M.: Development and Evaluation of a Convection Scheme for Use in Climate Models, Journal of the Atmospheric Sciences, 56, 1766–1782, https://doi.org/10.1175/1520-0469(1999)056<1766:DAEOAC>2.0.CO;2, 1999.

Ernle, L., Ringsdorf, M. A., and Williams, J.: Influence of ozone and humidity on PTR-MS and GC-MS VOC measurements with and without a $Na_2S_2O_3$ ozone scrubber, Atmospheric Measurement Techniques, 16, 1179–1194, https://doi.org/10.5194/amt-16-1179-2023, 2023.

Fall, R., Albritton, D. L., Fehsenfeld, F. C., Kuster, W. C., and Goldan, P. D.: Laboratory studies of some environmental variables controlling sulfur emissions from plants, Journal of Atmospheric Chemistry, 6, 341–362, https://doi.org/10.1007/BF00051596, 1988.

Fiddes, S. L., Woodhouse, M. T., Nicholls, Z., Lane, T. P., and Schofield, R.: Cloud, precipitation and radiation responses to large perturbations in global dimethyl sulfide, Atmospheric Chemistry and Physics, 18, 10 177–10 198, https://doi.org/10.5194/acp-18-10177-2018, 2018.

Filipy, J., Rumburg, B., Mount, G., Westberg, H., and Lamb, B.: Identification and quantification of volatile organic compounds from a dairy, Atmospheric Environment, 40, 1480–1494, https://doi.org/10.1016/j.atmosenv.2005.10.048, 2006.

Fraser, P. J., Dunse, B. L., Krummel, P. B., Steele, L. P., Derek, N., Mitrevski, B., Allison, C. E., Loh, Z., Manning, A. J., Redington, A., and Rigby, M.: Australian chlorofluorocarbon (CFC) emissions: 1960–2017, Environmental Chemistry, 17, 525–544, https://doi.org/10.1071/EN19322, 2020.

Fueglistaler, S., Wernli, H., and Peter, T.: Tropical troposphere-to-stratosphere transport inferred from trajectory calculations, Journal of Geophysical Research: Atmospheres, 109, https://doi.org/10.1029/2003JD004069, _eprint: https://agupubs.onlinelibrary.wiley.com/doi/pdf/10.1029/2003JD004069, 2004.

Galí, M., Levasseur, M., Devred, E., Simó, R., and Babin, M.: Sea-surface dimethylsulfide (DMS) concentration from satellite data at global and regional scales, Biogeosciences, 15, 3497–3519, https://doi.org/10.5194/bg-15-3497-2018, 2018.

Galí, M., Devred, E., Pérez, G. L., Kieber, D. J., and Simó, R.: Global Ocean dimethylsulfide photolysis rates quantified with a spectrally and vertically resolved model, Limnology and Oceanography Letters, 8, 760–769, https://doi.org/10.1002/lol2.10342, _eprint: https://aslopubs.onlinelibrary.wiley.com/doi/pdf/10.1002/lol2.10342, 2023.

Geng, C. and Mu, Y.: Carbonyl sulfide and dimethyl sulfide exchange between trees and the atmosphere, Atmospheric Environment, 40, 1373–1383, https://doi.org/10.1016/j.atmosenv.2005.10.023, 2006.

Giez, A., Zöger, M., Mallaun, C., Nenakhov, V., Schimpf, M., Grad, C., Numberger, A., and Raynor, K.: Determination of the Measurement Errors for the HALO Basic Data System BAHAMAS by Means of Error Propagation, Tech. rep., Deutsches Zentrum für Luft- und Raumfahrt (DLR), https://doi.org/10.57676/5RDC-Q708, 2022.

https://doi.org/10.5194/egusphere-2026-5595
Preprint. Discussion started: 22 September 2026

GTE Project Office, Anderson, B., Atlas, E., Bandy, A., Blake, D., Browell, E. V., Brune, W., Clarke, A., Davis, D., Eisele, F., Fuelberg, H., Gregory, G., Heikes, B., Mahoney, M. J., Owens, M., Ridley, B., Rodriguez, J., Sachse, G., Sandholm, S., Shetter, R., Singh, H., and Talbot, R.: PEM Tropics B Merge Data, https://doi.org/10.5067/ASDC/SUBORBITAL/PEM-TROPICS-B/MERGE_DATA_1, 2025.

Harazono, Y., Iwata, H., Sakabe, A., Ueyama, M., Takahashi, K., Nagano, H., Nakai, T., and Kosugi, Y.: Effects of water vapor dilution on trace gas flux, and practical correction methods, Journal of Agricultural Meteorology, 71, 65–76, https://doi.org/10.2480/agrmet.D-14-00003, 2015.

Hersbach, H., Bell, B., Berrisford, P., Hirahara, S., Horányi, A., Muñoz-Sabater, J., Nicolas, J., Peubey, C., Radu, R., Schepers, D., Simmons, A., Soci, C., Abdalla, S., Abellan, X., Balsamo, G., Bechtold, P., Biavati, G., Bidlot, J., Bonavita, M., De Chiara, G., Dahlgren, P., Dee, D., Diamantakis, M., Dragani, R., Flemming, J., Forbes, R., Fuentes, M., Geer, A., Haimberger, L., Healy, S., Hogan, R. J., Hólm, E., Janisková, M., Keeley, S., Laloyaux, P., Lopez, P., Lupu, C., Radnoti, G., de Rosnay, P., Rozum, I., Vamborg, F., Villaume, S., and Thépaut, J.-N.: The ERA5 global reanalysis, Quarterly Journal of the Royal Meteorological Society, 146, 1999–2049, https://doi.org/10.1002/qj.3803, _eprint: https://rmets.onlinelibrary.wiley.com/doi/pdf/10.1002/qj.3803, 2020.

Hoffmann, E. H., Tilgner, A., Schrödner, R., Bräuer, P., Wolke, R., and Herrmann, H.: An advanced modeling study on the impacts and atmospheric implications of multiphase dimethyl sulfide chemistry, Proceedings of the National Academy of Sciences, 113, 11 776–11 781, https://doi.org/10.1073/pnas.1606320113, 2016.

Hopkins, F. E., Archer, S. D., Bell, T. G., Suntharalingam, P., and Todd, J. D.: The biogeochemistry of marine dimethylsulfide, Nature Reviews Earth & Environment, 4, 361–376, https://doi.org/10.1038/s43017-023-00428-7, 2023.

Hulswar, S., Simó, R., Galí, M., Bell, T. G., Lana, A., Inamdar, S., Halloran, P. R., Manville, G., and Mahajan, A. S.: Third revision of the global surface seawater dimethyl sulfide climatology (DMS-Rev3), Earth System Science Data, 14, 2963–2987, https://doi.org/10.5194/essd-14-2963-2022, 2022.

Ingham, T., Bauer, D., Sander, R., Crutzen, P. J., and Crowley, J. N.: Kinetics and Products of the Reactions BrO + DMS and Br + DMS at 298 K, The Journal of Physical Chemistry A, 103, 7199–7209, https://doi.org/10.1021/jp9905979, 1999.

Jackson, R. L., Gabric, A. J., Woodhouse, M. T., Swan, H. B., Jones, G. B., Cropp, R., and Deschaseaux, E. S. M.: Coral Reef Emissions of Atmospheric Dimethylsulfide and the Influence on Marine Aerosols in the Southern Great Barrier Reef, Australia, Journal of Geophysical Research: Atmospheres, 125, e2019JD031 837, https://doi.org/10.1029/2019JD031837, _eprint: https://onlinelibrary.wiley.com/doi/pdf/10.1029/2019JD031837, 2020.

Jardine, K., Yañez-Serrano, A. M., Williams, J., Kunert, N., Jardine, A., Taylor, T., Abrell, L., Artaxo, P., Guenther, A., Hewitt, C. N., House, E., Florentino, A. P., Manzi, A., Higuchi, N., Kesselmeier, J., Behrendt, T., Veres, P. R., Derstroff, B., Fuentes, J. D., Martin, S. T., and Andreae, M. O.: Dimethyl sulfide in the Amazon rain forest, Global Biogeochemical Cycles, 29, 19–32, https://doi.org/10.1002/2014GB004969, 2015.

Jefferson, A., Nicovich, J. M., and Wine, P. H.: Temperature-Dependent Kinetics Studies of the Reactions Br(2P3/2) + CH3SCH3 .dblarw. CH3SCH2 + HBr. Heat of Formation of the CH3SCH2 Radical, The Journal of Physical Chemistry, 98, 7128–7135, https://doi.org/10.1021/j100080a006, 1994.

Jeuken, A. B. M., Siegmund, P. C., Heijboer, L. C., Feichter, J., and Bengtsson, L.: On the potential of assimilating meteorological analyses in a global climate model for the purpose of model validation, Journal of Geophysical Research: Atmospheres, 101, 16 939–16 950, https://doi.org/10.1029/96JD01218, _eprint: https://agupubs.onlinelibrary.wiley.com/doi/pdf/10.1029/96JD01218, 1996.

https://doi.org/10.5194/egusphere-2026-5595
Preprint. Discussion started: 22 September 2026

Joge, S. D., Mahajan, A. S., Hulswar, S., Marandino, C. A., Galí, M., Bell, T. G., and Simó, R.: Dimethyl sulfide (DMS) climatologies, fluxes, and trends – Part 1: Differences between seawater DMS estimations, Biogeosciences, 21, 4439–4452, https://doi.org/10.5194/bg-21-4439-2024, 2024.

Jöckel, P., Tost, H., Pozzer, A., Brühl, C., Buchholz, J., Ganzeveld, L., Hoor, P., Kerkweg, A., Lawrence, M. G., Sander, R., Steil, B., Stiller, G., Tanarhte, M., Taraborrelli, D., van Aardenne, J., and Lelieveld, J.: The atmospheric chemistry general circulation model ECHAM5/MESSy1: consistent simulation of ozone from the surface to the mesosphere, Atmospheric Chemistry and Physics, 6, 5067–5104, https://doi.org/10.5194/acp-6-5067-2006, 2006.

Jöckel, P., Kerkweg, A., Pozzer, A., Sander, R., Tost, H., Riede, H., Baumgaertner, A., Gromov, S., and Kern, B.: Development cycle 2 of the Modular Earth Submodel System (MESSy2), Geoscientific Model Development, 3, 717–752, https://doi.org/10.5194/gmd-3-717-2010, 2010.

Kammer, J., Décuq, C., Baisnée, D., Ciuraru, R., Lafouge, F., Buysse, P., Bsaibes, S., Henderson, B., Cristescu, S. M., Benabdallah, R., Chandra, V., Durand, B., Fanucci, O., Petit, J.-E., Truong, F., Bonnaire, N., Sarda-Estève, R., Gros, V., and Loubet, B.: Characterization of particulate and gaseous pollutants from a French dairy and sheep farm, Science of The Total Environment, 712, 135 598, https://doi.org/10.1016/j.scitotenv.2019.135598, 2020.

Kanda, K.-i., Tsuruta, H., and Minami, K.: Emission of dimethyl sulfide, carbonyl sulfide, and carbon bisulfide from paddy fields, Soil Science and Plant Nutrition, 38, 709–716, https://doi.org/10.1080/00380768.1992.10416701, _eprint: https://doi.org/10.1080/00380768.1992.10416701, 1992.

Kanda, K.-i., Tsuruta, H., and Minami, K.: Emissions of biogenic sulfur gases from maize and wheat fields, Soil Science and Plant Nutrition, 41, 1–8, https://doi.org/10.1080/00380768.1995.10419553, _eprint: https://doi.org/10.1080/00380768.1995.10419553, 1995.

Kesselmeier, J. and Hubert, A.: Exchange of reduced volatile sulfur compounds between leaf litter and the atmosphere, Atmospheric Environment, 36, 4679–4686, https://doi.org/10.1016/S1352-2310(02)00413-2, 2002.

Kettle, A. J., Andreae, M. O., Amouroux, D., Andreae, T. W., Bates, T. S., Berresheim, H., Bingemer, H., Boniforti, R., Curran, M. A. J., DiTullio, G. R., Helas, G., Jones, G. B., Keller, M. D., Kiene, R. P., Leck, C., Levasseur, M., Malin, G., Maspero, M., Matrai, P., McTaggart, A. R., Mihalopoulos, N., Nguyen, B. C., Novo, A., Putaud, J. P., Rapsomanikis, S., Roberts, G., Schebeske, G., Sharma, S., Simó, R., Staubes, R., Turner, S., and Uher, G.: A global database of sea surface dimethylsulfide (DMS) measurements and a procedure to predict sea surface DMS as a function of latitude, longitude, and month, Global Biogeochemical Cycles, 13, 399–444, https://doi.org/10.1029/1999GB900004, 1999.

Kim, K.-H., Shon, Z.-H., Nguyen, H. T., and Jeon, E.-C.: A review of major chlorofluorocarbons and their halocarbon alternatives in the air, Atmospheric Environment, 45, 1369–1382, https://doi.org/10.1016/j.atmosenv.2010.12.029, 2011.

Kley, D., Crutzen, P. J., Smit, H. G. J., Vömel, H., Oltmans, S. J., Grassl, H., and Ramanathan, V.: Observations of Near-Zero Ozone Concentrations Over the Convective Pacific: Effects on Air Chemistry, Science, 274, 230–233, https://doi.org/10.1126/science.274.5285.230, 1996.

Kohl, M., Lelieveld, J., Chowdhury, S., Ehrhart, S., Sharma, D., Cheng, Y., Tripathi, S. N., Sebastian, M., Pandithurai, G., Wang, H., and Pozzer, A.: Numerical simulation and evaluation of global ultrafine particle concentrations at the Earth's surface, Atmospheric Chemistry and Physics, 23, 13 191–13 215, https://doi.org/10.5194/acp-23-13191-2023, 2023.

Korhonen, H., Carslaw, K. S., Spracklen, D. V., Mann, G. W., and Woodhouse, M. T.: Influence of oceanic dimethyl sulfide emissions on cloud condensation nuclei concentrations and seasonality over the remote Southern Hemisphere oceans:

https://doi.org/10.5194/egusphere-2026-5595
Preprint. Discussion started: 22 September 2026

A global model study, Journal of Geophysical Research: Atmospheres, 113, https://doi.org/10.1029/2007JD009718, _eprint: https://agupubs.onlinelibrary.wiley.com/doi/pdf/10.1029/2007JD009718, 2008.

Lana, A., Bell, T. G., Simó, R., Vallina, S. M., Ballabrera-Poy, J., Kettle, A. J., Dachs, J., Bopp, L., Saltzman, E. S., Stefels, J., Johnson, J. E., and Liss, P. S.: An updated climatology of surface dimethlysulfide concentrations and emission fluxes in the global ocean: UPDATED DMS CLIMATOLOGY, Global Biogeochemical Cycles, 25, n/a–n/a, https://doi.org/10.1029/2010GB003850, 2011.

Leck, C. and Persson, C.: Seasonal and short-term variability in dimethyl sulfide, sulfur dioxide and biogenic sulfur and sea salt aerosol particles in the arctic marine boundary layer during summer and autumn, Tellus B: Chemical and Physical Meteorology, 48, 272–299, https://doi.org/10.3402/tellusb.v48i2.15891, _eprint: https://doi.org/10.3402/tellusb.v48i2.15891, 1996.

Li, J., Shen, L., Zhang, Y., Liu, Y., Wu, J., and Wang, A.: Carbonyl Sulfide (COS) in Terrestrial Ecosystem: What We Know and What We Do Not, Atmosphere, 15, 778, https://doi.org/10.3390/atmos15070778, 2024.

Liss, P. S. and Slater, P. G.: Flux of Gases across the Air-Sea Interface, Nature, 247, 181–184, https://doi.org/10.1038/247181a0, 1974.

Loubet, B., Buysse, P., Gonzaga-Gomez, L., Lafouge, F., Ciuraru, R., Decuq, C., Kammer, J., Bsaibes, S., Boissard, C., Durand, B., Gueudet, J.-C., Fanucci, O., Zurfluh, O., Abis, L., Zannoni, N., Truong, F., Baisnée, D., Sarda-Estève, R., Staudt, M., and Gros, V.: Volatile organic compound fluxes over a winter wheat field by PTR-Qi-TOF-MS and eddy covariance, Atmospheric Chemistry and Physics, 22, 2817–2842, https://doi.org/10.5194/acp-22-2817-2022, 2022.

Machado, L. A. T., Laurent, H., Dessay, N., and Miranda, I.: Seasonal and diurnal variability of convection over the Amazonia: A comparison of different vegetation types and large scale forcing, Theoretical and Applied Climatology, 78, 61–77, https://doi.org/10.1007/s00704-004-0044-9, 2004.

Marandino, C. A., Tegtmeier, S., Krüger, K., Zindler, C., Atlas, E. L., Moore, F., and Bange, H. W.: Dimethylsulphide (DMS) emissions from the western Pacific Ocean: a potential marine source for stratospheric sulphur?, Atmospheric Chemistry and Physics, 13, 8427–8437, https://doi.org/10.5194/acp-13-8427-2013, 2013.

Mesarchaki, E., Kräuter, C., Krall, K. E., Bopp, M., Helleis, F., Williams, J., and Jähne, B.: Measuring air–sea gas-exchange velocities in a large-scale annular wind–wave tank, Ocean Science, 11, 121–138, https://doi.org/10.5194/os-11-121-2015, 2015.

Miller, B. R., Weiss, R. F., Salameh, P. K., Tanhua, T., Greally, B. R., Mühle, J., and Simmonds, P. G.: Medusa: a sample preconcentration and GC/MS detector system for in situ measurements of atmospheric trace halocarbons, hydrocarbons, and sulfur compounds, Analytical Chemistry, 80, 1536–1545, https://doi.org/10.1021/ac702084k, 2008.

Montzka, S. A., Butler, J. H., Elkins, J., Thompson, T. M., Clarke, A. D., and Lock, L. T.: Present and future trends in the atmospheric burden of ozone-depleting halogens, Nature, 398, 690–694, https://doi.org/10.1038/19499, 1999.

Myhre, G., Samset, B. H., Schulz, M., Balkanski, Y., Bauer, S., Berntsen, T. K., Bian, H., Bellouin, N., Chin, M., Diehl, T., Easter, R. C., Feichter, J., Ghan, S. J., Hauglustaine, D., Iversen, T., Kinne, S., Kirkevåg, A., Lamarque, J.-F., Lin, G., Liu, X., Lund, M. T., Luo, G., Ma, X., van Noije, T., Penner, J. E., Rasch, P. J., Ruiz, A., Seland, O., Skeie, R. B., Stier, P., Takemura, T., Tsigaridis, K., Wang, P., Wang, Z., Xu, L., Yu, H., Yu, F., Yoon, J.-H., Zhang, K., Zhang, H., and Zhou, C.: Radiative forcing of the direct aerosol effect from AeroCom Phase II simulations, Atmospheric Chemistry and Physics, 13, 1853–1877, https://doi.org/10.5194/acp-13-1853-2013, 2013.

Nordeng, T.-E.: Extended versions of the convective parametrization scheme at ECMWF and their impact on the mean and transient activity of the model in the tropics, Tech. Rep., 206, https://doi.org/10.21957/E34XWHYSW, 1994.

Novak, G. A., Fite, C. H., Holmes, C. D., Veres, P. R., Neuman, J. A., Faloona, I., Thornton, J. A., Wolfe, G. M., Vermeuel, M. P., Jernigan, C. M., Peischl, J., Ryerson, T. B., Thompson, C. R., Bourgeois, I., Warneke, C., Gkatzelis, G. I., Coggon, M. M., Sekimoto, K., Bui, T. P., Dean-Day, J., Diskin, G. S., DiGangi, J. P., Nowak, J. B., Moore, R. H., Wiggins, E. B., Winstead, E. L., Robinson, C., Thornhill,

https://doi.org/10.5194/egusphere-2026-5595
Preprint. Discussion started: 22 September 2026

K. L., Sanchez, K. J., Hall, S. R., Ullmann, K., Dollner, M., Weinzierl, B., Blake, D. R., and Bertram, T. H.: Rapid cloud removal of dimethyl sulfide oxidation products limits SO_2 and cloud condensation nuclei production in the marine atmosphere, Proceedings of the National Academy of Sciences, 118, e2110472 118, https://doi.org/10.1073/pnas.2110472118, company: National Academy of Sciences Distributor: National Academy of Sciences Institution: National Academy of Sciences Label: National Academy of Sciences, 2021.

Nowak, J. B., Davis, D. D., Chen, G., Eisele, F. L., Mauldin, R. L., Tanner, D. J., Cantrell, C., Kosciuch, E., Bandy, A., Thornton, D., and Clarke, A.: Airborne observations of DMSO, DMS, and OH at marine tropical latitudes, Geophysical Research Letters, 28, 2201–2204, https://doi.org/10.1029/2000GL012297, 2001.

Nussbaumer, C. M., Pozzer, A., Hewson, M., Ort, L., Krumm, B., Byron, J., Williams, J., Joppe, P., Obersteiner, F., Zahn, A., Lelieveld, J., and Fischer, H.: Low Tropospheric Ozone Over the Indo-Pacific Warm Pool Related to Non-Electrified Convection, Geophysical Research Letters, 52, e2024GL112 788, https://doi.org/10.1029/2024GL112788, _eprint: https://onlinelibrary.wiley.com/doi/pdf/10.1029/2024GL112788, 2025.

Pope, M., Jakob, C., and Reeder, M. J.: Convective Systems of the North Australian Monsoon, Journal of Climate, 21, 5091–5112, https://doi.org/10.1175/2008JCLI2304.1, 2008.

Pozzer, A., Jöckel, P., Sander, R., Williams, J., Ganzeveld, L., and Lelieveld, J.: Technical Note: The MESSy-submodel AIRSEA calculating the air-sea exchange of chemical species, Atmospheric Chemistry and Physics, 6, 5435–5444, https://doi.org/10.5194/acp-6-5435-2006, 2006.

Prinn, R., Weiss, R., Arduini, J., Choi, H., Engel, A., Fraser, P., Ganesan, A., Harth, C., Hermansen, O., Kim, J., Krummel, P., Loh, Z., Lunder, C., Maione, M., Manning, A., Mitrevski, B., Mühle, J., O'Doherty, S., Park, S., Pitt, J., Reimann, S., Rigby, M., Saito, T., Salameh, P., Schmidt, R., Simmonds, P., Stanley, K., Stavert, A., Steele, P., Vollmer, M., Wagenhäuser, T., Wang, H., Wenger, A., Western, L., Yao, B., Young, D., Zhou, L., and Zhu, L.: The dataset of in-situ measurements of chemically and radiatively important atmospheric gases from the Advanced Global Atmospheric Gas Experiment (AGAGE) and affiliated stations, https://doi.org/10.60718/75D7-QE84, 2025.

Prinn, R. G., Weiss, R. F., Arduini, J., Arnold, T., DeWitt, H. L., Fraser, P. J., Ganesan, A. L., Gasore, J., Harth, C. M., Hermansen, O., Kim, J., Krummel, P. B., Li, S., Loh, Z. M., Lunder, C. R., Maione, M., Manning, A. J., Miller, B. R., Mitrevski, B., Mühle, J., O'Doherty, S., Park, S., Reimann, S., Rigby, M., Saito, T., Salameh, P. K., Schmidt, R., Simmonds, P. G., Steele, L. P., Vollmer, M. K., Wang, R. H., Yao, B., Yokouchi, Y., Young, D., and Zhou, L.: History of chemically and radiatively important atmospheric gases from the Advanced Global Atmospheric Gases Experiment (AGAGE), Earth System Science Data, 10, 985–1018, https://doi.org/10.5194/essd-10-985-2018, 2018.

Pugliese, G., Ingrisch, J., Meredith, L. K., Pfannerstill, E. Y., Klüpfel, T., Meeran, K., Byron, J., Purser, G., Gil-Loaiza, J., van Haren, J., Dontsova, K., Kreuzwieser, J., Ladd, S. N., Werner, C., and Williams, J.: Effects of drought and recovery on soil volatile organic compound fluxes in an experimental rainforest, Nature Communications, 14, 5064, https://doi.org/10.1038/s41467-023-40661-8, 2023.

Pöhlker, C., Walter, D., Paulsen, H., Könemann, T., Rodríguez-Caballero, E., Moran-Zuloaga, D., Brito, J., Carbone, S., Degrendele, C., Després, V. R., Ditas, F., Holanda, B. A., Kaiser, J. W., Lammel, G., Lavrič, J. V., Ming, J., Pickersgill, D., Pöhlker, M. L., Praß, M., Löbs, N., Saturno, J., Sörgel, M., Wang, Q., Weber, B., Wolff, S., Artaxo, P., Pöschl, U., and Andreae, M. O.: Land cover and its transformation in the backward trajectory footprint region of the Amazon Tall Tower Observatory, Atmospheric Chemistry and Physics, 19, 8425–8470, https://doi.org/10.5194/acp-19-8425-2019, 2019.

Pöschl, U., von Kuhlmann, R., Poisson, N., and Crutzen, P. J.: Development and Intercomparison of Condensed Isoprene Oxidation Mechanisms for Global Atmospheric Modeling, Journal of Atmospheric Chemistry, 37, 29–52, https://doi.org/10.1023/A:1006391009798, 2000.

Quinn, P. K. and Bates, T. S.: The case against climate regulation via oceanic phytoplankton sulphur emissions, Nature, 480, 51–56, https://doi.org/10.1038/nature10580, 2011.

https://doi.org/10.5194/egusphere-2026-5595
Preprint. Discussion started: 22 September 2026

Rasmussen, F. R., Kubečka, J., and Elm, J.: Contribution of Methanesulfonic Acid to the Formation of Molecular Clusters in the Marine Atmosphere, The Journal of Physical Chemistry A, 126, 7127–7136, https://doi.org/10.1021/acs.jpca.2c04468, 2022.

Rennenberg, H.: The Fate of Excess Sulfur in Higher Plants, Annual Review of Plant Physiology, 35, 121–153, https://doi.org/10.1146/annurev.pp.35.060184.001005, 1984.

Rex, M., Wohltmann, I., Ridder, T., Lehmann, R., Rosenlof, K., Wennberg, P., Weisenstein, D., Notholt, J., Krüger, K., Mohr, V., and Tegtmeier, S.: A tropical West Pacific OH minimum and implications for stratospheric composition, Atmospheric Chemistry and Physics, 14, 4827–4841, https://doi.org/10.5194/acp-14-4827-2014, 2014.

Roeckner, E., Brokopf, R., Esch, M., Giorgetta, M., Hagemann, S., Kornblueh, L., Manzini, E., Schlese, U., and Schulzweida, U.: Sensitivity of Simulated Climate to Horizontal and Vertical Resolution in the ECHAM5 Atmosphere Model, Journal of Climate, 19, 3771–3791, https://doi.org/10.1175/JCLI3824.1, 2006.

Rybka, H. and Tost, H.: Uncertainties in future climate predictions due to convection parameterisations, Atmospheric Chemistry and Physics, 14, 5561–5576, https://doi.org/10.5194/acp-14-5561-2014, 2014.

Salignat, R., Rose, C., Banson, S., Berthet, S., Lupascu, A., Uitz, J., Mallet, M., Seferian, R., Rocco, M., Colomb, A., Dunne, E., Saint-Macary, A., Marriner, A., Law, C. S., and Sellegri, K.: Sensitivity Study of Atmospheric DMS Simulated in WRF-Chem to Various Oceanic DMS Fields Over the South West Pacific, Journal of Geophysical Research: Atmospheres, 130, e2024JD042 271, https://doi.org/10.1029/2024JD042271, _eprint: https://agupubs.onlinelibrary.wiley.com/doi/pdf/10.1029/2024JD042271, 2025.

Sanchez, K. J., Chen, C.-L., Russell, L. M., Betha, R., Liu, J., Price, D. J., Massoli, P., Ziemba, L. D., Crosbie, E. C., Moore, R. H., Müller, M., Schiller, S. A., Wisthaler, A., Lee, A. K. Y., Quinn, P. K., Bates, T. S., Porter, J., Bell, T. G., Saltzman, E. S., Vaillancourt, R. D., and Behrenfeld, M. J.: Substantial Seasonal Contribution of Observed Biogenic Sulfate Particles to Cloud Condensation Nuclei, Scientific Reports, 8, 3235, https://doi.org/10.1038/s41598-018-21590-9, 2018.

Sander, R., Baumgaertner, A., Cabrera-Perez, D., Frank, F., Gromov, S., Grooß, J.-U., Harder, H., Huijnen, V., Jöckel, P., Karydis, V. A., Niemeyer, K. E., Pozzer, A., Riede, H., Schultz, M. G., Taraborrelli, D., and Tauer, S.: The community atmospheric chemistry box model CAABA/MECCA-4.0, Geoscientific Model Development, 12, 1365–1385, https://doi.org/10.5194/gmd-12-1365-2019, 2019.

Shaw, G. E.: Bio-controlled thermostasis involving the sulfur cycle, Climatic Change, 5, 297–303, https://doi.org/10.1007/BF02423524, 1983.

Shaw, S. L., Mitloehner, F. M., Jackson, W., DePeters, E. J., Fadel, J. G., Robinson, P. H., Holzinger, R., and Goldstein, A. H.: Volatile Organic Compound Emissions from Dairy Cows and Their Waste as Measured by Proton-Transfer-Reaction Mass Spectrometry, Environmental Science & Technology, 41, 1310–1316, https://doi.org/10.1021/es061475e, 2007.

Simpson, I. J., Colman, J. J., Swanson, A. L., Bandy, A. R., Thornton, D. C., Blake, D. R., and Rowland, F. S.: Aircraft Measurements of Dimethyl Sulfide (DMS) Using a Whole Air Sampling Technique, Journal of Atmospheric Chemistry, 39, 191–213, https://doi.org/10.1023/A:1010608529779, 2001.

Simó, R., Hatton*, A. D., Malin, G., and Liss, P. S.: Particulate dimethyl sulphoxide in seawater: production by microplankton, Marine Ecology Progress Series, 167, 291–296, https://doi.org/10.3354/meps167291, 1998.

Sipilä, M., Berndt, T., Petäjä, T., Brus, D., Vanhanen, J., Stratmann, F., Patokoski, J., Mauldin, R. L., Hyvärinen, A.-P., Lihavainen, H., and Kulmala, M.: The Role of Sulfuric Acid in Atmospheric Nucleation, Science, 327, 1243–1246, https://doi.org/10.1126/science.1180315, 2010.

Spiro, P. A., Jacob, D. J., and Logan, J. A.: Global inventory of sulfur emissions with 1°×1° resolution, Journal of Geophysical Research: Atmospheres, 97, 6023–6036, https://doi.org/10.1029/91JD03139, 1992.

https://doi.org/10.5194/egusphere-2026-5595
Preprint. Discussion started: 22 September 2026

Staubes, R., Georgii, H.-W., and Ockelmann, G.: Flux of COS, DMS and CS2 from various soils in Germany, Tellus B, 41B, 305–313, https://doi.org/10.1111/j.1600-0889.1989.tb00309.x, _eprint: https://onlinelibrary.wiley.com/doi/pdf/10.1111/j.1600-0889.1989.tb00309.x, 1989.

Stein, A. F., Draxler, R. R., Rolph, G. D., Stunder, B. J. B., Cohen, M. D., and Ngan, F.: NOAA's HYSPLIT Atmospheric Transport and Dispersion Modeling System, Bulletin of the American Meteorological Society, 96, 2059–2077, https://doi.org/10.1175/BAMS-D-14-00110.1, 2015.

Thornton, D. C., Bandy, A. R., Blomquist, B. W., Bradshaw, J. D., and Blake, D. R.: Vertical transport of sulfur dioxide and dimethyl sulfide in deep convection and its role in new particle formation, Journal of Geophysical Research: Atmospheres, 102, 28 501–28 509, https://doi.org/10.1029/97JD01647, _eprint: https://agupubs.onlinelibrary.wiley.com/doi/pdf/10.1029/97JD01647, 1997.

Tiedtke, M.: A Comprehensive Mass Flux Scheme for Cumulus Parameterization in Large-Scale Models, Monthly Weather Review, 117, 1779–1800, https://doi.org/10.1175/1520-0493(1989)117<1779:ACMFSF>2.0.CO;2, 1989.

Tost, H., Jöckel, P., and Lelieveld, J.: Influence of different convection parameterisations in a GCM, Atmospheric Chemistry and Physics, 6, 5475–5493, https://doi.org/10.5194/acp-6-5475-2006, 2006.

Tripathi, N., E. Krumm, B., Edtbauer, A., Ringsdorf, A., Wang, N., Kohl, M., Vella, R., Machado, L. A. T., Pozzer, A., Lelieveld, J., and Williams, J.: Impacts of convection, chemistry, and forest clearing on biogenic volatile organic compounds over the Amazon, https://doi.org/10.6084/M9.FIGSHARE.28692260, artwork Size: 4817887 Bytes Pages: 4817887 Bytes, 2025.

Tuomisto, H., Van doninck, J., Ruokolainen, K., Moulatlet, G. M., Figueiredo, F. O. G., Sirén, A., Cárdenas, G., Lehtonen, S., and Zuquim, G.: Discovering floristic and geoecological gradients across Amazonia, Journal of Biogeography, 46, 1734–1748, https://doi.org/10.1111/jbi.13627, _eprint: https://onlinelibrary.wiley.com/doi/pdf/10.1111/jbi.13627, 2019.

Vermeuel, M. P., Novak, G. A., Kilgour, D. B., Claflin, M. S., Lerner, B. M., Trowbridge, A. M., Thom, J., Cleary, P. A., Desai, A. R., and Bertram, T. H.: Observations of biogenic volatile organic compounds over a mixed temperate forest during the summer to autumn transition, Atmospheric Chemistry and Physics, 23, 4123–4148, https://doi.org/10.5194/acp-23-4123-2023, 2023.

Vettikkat, L., Sinha, V., Datta, S., Kumar, A., Hakkim, H., Yadav, P., and Sinha, B.: Significant emissions of dimethyl sulfide and monoterpenes by big-leaf mahogany trees: discovery of a missing dimethyl sulfide source to the atmospheric environment, Atmospheric Chemistry and Physics, 20, 375–389, https://doi.org/10.5194/acp-20-375-2020, 2020.

Voigt, C., Lelieveld, J., Schlager, H., Schneider, J., Curtius, J., Meerkötter, R., Sauer, D., Bugliaro, L., Bohn, B., Crowley, J. N., Erbertseder, T., Groß, S., Hahn, V., Li, Q., Mertens, M., Pöhlker, M. L., Pozzer, A., Schumann, U., Tomsche, L., Williams, J., Zahn, A., Andreae, M., Borrmann, S., Bräuer, T., Dörich, R., Dörnbrack, A., Edtbauer, A., Ernle, L., Fischer, H., Giez, A., Granzin, M., Grewe, V., Harder, H., Heinritzi, M., Holanda, B. A., Jöckel, P., Kaiser, K., Krüger, O. O., Lucke, J., Marsing, A., Martin, A., Matthes, S., Pöhlker, C., Pöschl, U., Reifenberg, S., Ringsdorf, A., Scheibe, M., Tadic, I., Zauner-Wieczorek, M., Henke, R., and Rapp, M.: Cleaner Skies during the COVID-19 Lockdown, Bulletin of the American Meteorological Society, 103, E1796–E1827, https://doi.org/10.1175/BAMS-D-21-0012.1, 2022.

Wang, S., Apel, E. C., Schwantes, R. H., Bates, K. H., Jacob, D. J., Fischer, E. V., Hornbrook, R. S., Hills, A. J., Emmons, L. K., Pan, L. L., Honomichl, S., Tilmes, S., Lamarque, J., Yang, M., Marandino, C. A., Saltzman, E. S., de Bruyn, W., Kameyama, S., Tanimoto, H., Omori, Y., Hall, S. R., Ullmann, K., Ryerson, T. B., Thompson, C. R., Peischl, J., Daube, B. C., Commane, R., McKain, K., Sweeney, C., Thames, A. B., Miller, D. O., Brune, W. H., Diskin, G. S., DiGangi, J. P., and Wofsy, S. C.: Global Atmospheric Budget of Acetone: Air-Sea Exchange and the Contribution to Hydroxyl Radicals, Journal of Geophysical Research: Atmospheres, 125, https://doi.org/10.1029/2020JD032553, 2020.

https://doi.org/10.5194/egusphere-2026-5595
Preprint. Discussion started: 22 September 2026

Watts, S. F.: The mass budgets of carbonyl sulfide, dimethyl sulfide, carbon disulfide and hydrogen sulfide, Atmospheric Environment, 34, 761–779, https://doi.org/10.1016/S1352-2310(99)00342-8, 2000.

Williams, J., Wang, N.-Y., Cicerone, R. J., Yagi, K., Kurihara, M., and Terada, F.: Atmospheric methyl halides and dimethyl sulfide from cattle, Global Biogeochemical Cycles, 13, 485–491, https://doi.org/10.1029/1998GB900010, _eprint: https://agupubs.onlinelibrary.wiley.com/doi/pdf/10.1029/1998GB900010, 1999.

Williams, J., Fischer, H., Hoor, P., Pöschl, U., Crutzen, P., Andreae, M., and Lelieveld, J.: The influence of the tropical rainforest on atmospheric CO and CO2 as measured by aircraft over Surinam, South America, Chemosphere - Global Change Science, 3, 157–170, https://doi.org/10.1016/S1465-9972(00)00047-7, 2001.

Williams, J., Holzinger, R., Gros, V., Xu, X., Atlas, E., and Wallace, D. W. R.: Measurements of organic species in air and seawater from the tropical Atlantic, Geophysical Research Letters, 31, https://doi.org/10.1029/2004GL020012, _eprint: https://agupubs.onlinelibrary.wiley.com/doi/pdf/10.1029/2004GL020012, 2004.

Yang, G.-Y. and Slingo, J.: The Diurnal Cycle in the Tropics, Monthly Weather Review, 129, 784–801, https://doi.org/10.1175/1520-0493(2001)129<0784:TDCITT>2.0.CO;2, 2001.

Yonemura, S., Sandoval-Soto, L., Kesselmeier, J., Kuhn, U., Von Hobe, M., Yakir, D., and Kawashima, S.: Uptake of carbonyl sulfide (COS) and emission of dimethyl sulfide (DMS) by plants, Phyton-Annales Rei Botanicae, 45, 17–24, 2005.

Zeng, X., Wang, W., Liu, C., Shan, C., Xie, Y., Wu, P., Zhu, Q., Zhou, M., De Mazière, M., Mahieu, E., Pardo Cantos, I., Makkor, J., and Polyakov, A.: Retrieval of atmospheric CFC-11 and CFC-12 from high-resolution FTIR observations at Hefei and comparisons with other independent datasets, Atmospheric Measurement Techniques, 15, 6739–6754, https://doi.org/10.5194/amt-15-6739-2022, 2022.

Zhou, S., Chen, Y., Huang, S., Gong, X., Yang, G., Zhang, H., Herrmann, H., Wiedensohler, A., Poulain, L., Zhang, Y., Wang, F., Xu, Z., and Yan, K.: A 20-year (1998–2017) global sea surface dimethyl sulfide gridded dataset with daily resolution, Earth System Science Data, 16, 4267–4290, https://doi.org/10.5194/essd-16-4267-2024, 2024.